D-MEM
PhD-UNIMI

Doctorate program
Milan
EXPERIMENTAL
MEDICINE

Università degli Studi di Milano

PhD Course in
Experimental Medicine

CYCLE XXXIV

PhD thesis

VOLTAGE GATED SODIUM CHANNEL AND NEURONAL DIFFERENTIATION. IMPLICATIONS IN AMYOTROPHIC LATERAL SCLEROSIS PATHOGENESIS

Candidate: **Dr. Maria Nicol Colombo**
Matr. R12270

Tutor: **Prof. Maura Francolini**

Director: **Prof. Nicoletta Landsberger**

Academic Year 2021-2022

Abstract

Voltage gated sodium channels (VGSCs) are multimeric protein complexes formed by one alpha subunit, responsible of pore formation and of the regulation of the state of the channel, and by one or two accessory beta subunits that have an important role in the regulation of alpha subunit localization and kinetics and in the interaction with the extracellular environment. VGSCs, together with Calcium and Potassium voltage dependent channels, are involved in the definition of cellular electrical properties. In particular, a small percentage (1%) of the voltage dependent Na^+ current generated by VGSCs is a non-inactivating component (Persistent Sodium Current, I_{NaP}).

Recent evidence pointed out an involvement of VGSCs and I_{NaP} in promoting neurite elongation in health and disease. Indeed, Na_V 1.6 and β1 subunits were reported to be fundamental in axonal outgrowth in mouse neuron primary culture. Moreover, our previous studies on a zebrafish model of Amyotrophic Lateral Sclerosis, that express the mutant G93R form of the superoxide dismutase 1 (SOD1) enzyme, show that alteration in the I_{NaP} of spinal inter- and moto- neurons induced neuron hyperexcitability that finally leads to hyperactive zebrafish locomotor behaviour together with morphological alterations of motoneuronal phenotype.

In this scenario, we decided to deeper investigate the role of VGSCs in neurite elongation, by taking advantage of the NSC34 cell line, an *in vitro* model often used in the study of motoneuron disease. Thus, we used two different NSC34 model of ALS, the first one expressing the human wild-type (WT) or G93A form of the SOD1 enzyme and the second one that lacks for the expression of the vesicle-associated membrane protein associated protein B (VAPB) protein.

By mean of different experimental approaches we study the expression of VGSCs protein and mRNA levels, the localization of the channel and the ability of the cell to respond to a depolarizing stimulus in health and disease *in vitro* models. Then, taking advantage of pharmacological approaches we evaluate whether changes in VGSCs functionality cause impairments in neurites elongation.

Surprisingly, we found a strong correlation between VGSCs expression, localization and functionality and neuron differentiation in all the model we analysed. In particular, VGSCs increased expression seems to be functional to the increase in the percentage of differentiated cells during NSC34 differentiation. Moreover, NSC34 defective neurite outgrowth correlates with VGSCs defective expression or localization in NSC34 ALS models.

In conclusion, the study that I have conduct during the three years of my PhD project point out an interesting correlation between VGSCs and motoneuron differentiation with possible implication in ALS pathogenesis.

Disclosure for research integrity

Data presented in this thesis are obtained and analysed following the principles of research integrity with Rigour, Honesty and Integrity. The Material and Methods section describe precisely how experiments were carried out in order to allow other scientist to replicate the experiments.

The statistical test used, and relative corrections are described in the Material and Methods section.

For blot experiments, all the samples of the same experiments were run in the same electrophoretic gel as well as the loading controls.

For immunofluorescence experiments, all the sample of an experiment were processed simultaneously, and random field images were acquired maintaining the same parameters. When image processing was needed, the same adjustments were applied to all the images of the experiment.

Abbreviations

- AIS: Axon Initial Segment
- ALS: Amyotrophic Lateral Sclerosis
- BCA: Bicinconinic Acid
- BB1: Blocking Buffer 1
- BB2: Blocking Buffer 2
- BSA: Bovine Serum Albumin
- C9orf72: chromosome 9 open reading frame 72
- CNS: Central nervous system
- CNX: Calnexin
- DAPI: 4,6-diamidino-2-phenylindole
- DisBaC2(3): Bis-(1,3-Diethylthiobarbituric Acid) Trimethine Oxonol
- DMEM: Dulbecco's modified Eagle medium
- ER: Endoplasmic Reticulum
- fALS: familial ALS
- FBS: Fetal Bovine Serum
- FDA: Food and Drug Administration
- FUS: Fused in Sarcoma
- G418: Geneticin
- GAP43: Growth Associated Protein 43
- GSDB: Goat Serum Diliution Buffer
- HCN: Hyperpolarization-activated cyclic nucleotide-gated channel
- hpf: Hours post-fertilization
- HS-PBS: High Salt Phosphate Buffer Saline
- IF: Immunofluorescence
- I_{NaP}: Persistent sodium current
- i.p.: protease inhibitor
- LS-PBS: low-salt Phosphate Buffer Saline
- MSP: Major Sperm Protein
- NEAA : Non-Essential Amino Acids
- NT: Non-Transfected
- ON: Overnight

- OSBP: Oxysterol-binding protein
- PBS: Phosphate Buffered Saline
- PI: Phosphoinositides
- PI4P: Phosphatidylinositol 4-phosphate
- PKA: Protein Kinase A
- PKC: Protein kinase C
- RA: Retinoic Acid
- RB: Rohon-Beard
- ROS: Reactive oxygen species
- RT: Room Temperature
- SDS: Sodium Dodecyl Sulfate
- sALS: sporadic ALS
- SD: Standard Deviation
- S.E.M.: Standard Error of the Mean
- sh: short hairpin
- SOD1: superoxide dismutase 1
- TARDBP: TAR DNA-binding protein 43
- TDP-43: TAR DNA-binding protein 43
- TBS: Tris-Buffered-Saline
- TTX: Tetrodotoxin
- SOD1: superoxide dismutase 1
- Tub: Tubulin
- UBQLN2: Ubiquilin-2
- UD: Undifferentiated
- UPR: Unfolded Protein Response
- VGSC: Voltage Gated Sodium Channel
- VAPB: Vesicle associated membrane protein associated protein B
- WB: Western Blotting
- WT: wild-type

Introduction

Voltage Gated Sodium Channel

Voltage gated sodium channels (VGSCs) are multimeric protein complexes that, together with potassium and calcium voltage dependent channels, are essential to define the electrical proprieties of depolarizing cells (1, 2).

In neurons, VGSCs generate a voltage-dependent sodium current that involves a transient inward flux of Na^+ that depolarizes cell membrane and mediate the upstroke and propagation of the action potential. A non-inactivating component of the total sodium current, the persistent sodium current (I_{NaP}), affects neurons excitability and accounts for about the 1% of the peak inward sodium current. Since the voltage range in which I_{NaP} is activated is in between two spikes of the action potential, a small increase of it can facilitate repetitive firing leading to hyperexcitability (3). Thus, despite I_{NaP} represent a small fraction of the total sodium current, its alteration can affect cell firing behavior profoundly (4).

VGSC protein complex is made by one alpha subunit, essential for the formation of the pore and the regulation of the state of the channel (open, close and inactive) and one or two beta subunits that are involved in the adhesion with extracellular environment and regulate both the localization and kinetics of the channel (5, 6). In mammals 9 different alpha and 4 different beta subunits are differentially express during life. In particular, all the 4 β subunits are expressed in the Central Nervous System (CNS) (7) with the β1b and β3 subunits expressed in the early stage of development and β1 an β2 in the adulthood (8, 9). Among the 9 α subunits, 5 ($Na_V1.1$, $Na_V1.2$, $Na_V1.3$, $Na_V1.5$, $Na_V1.8$) are expressed during CNS development with a fine spatial-temporal regulation (Table 1).

α-subunit

The α-subunit of the channel is a highly glycosylated 240-280 kDa transmembrane protein made by six transmembrane α-helices (S1-S6) repeated in four domains (I-IV) with the N- and C- terminal tails in the intracellular space (10). The interior of the pore is made up of the amino acid residues of the S6 helices, while the intracellular part of the pore is made up of the loops that connect the four domains.

The voltage sensor of the channel is made by the sequence of positive and hydrophobic amino acid residues in the fourth α-helices of each domain (S4) while the selectivity filter for Na^+ ions are made by the sequence of negatively charges amino acid in the loop connecting the S5 and S6 helices of each domain (11). The depolarization of the membrane determines the outward movement of the S4 helix, causing a conformational change that induces the opening of the pore. The inactivation domain is composed by a conserved idrofobic Ile-Phe-Met sequence (IFM motif) found at the level of the intracellular loop between the III and the IV domain that prevent the entry of ions (10, 12, 13).

β-subunit

The 4 different β-subunits that bind covalently, through cysteine bonds (β2 and β4), or non-covalently (β1 and β3) the α-subunit (14, 15) are 33-39 kDa transmembrane proteins with a small intracellular C-terminal domain, a transmembrane domain, and an N-terminal Ig like, highly glycosylated extracellular domain (13). In addition to being important in the modulation of the kinetics of the α subunit (16), β subunits are also important in the interaction with the extracellular environment. Thus, the adhesion motif in the N-terminal domain of the protein interacts with the extracellular matrix and glial cells regulating neurite outgrowth and Ranvier nodes maintenance (12, 17, 18). In particular, β1 and β1b subunit seems to be important in promoting neurite outgrowth, conversely the β2 has an inhibitor effect in neurite elongation (19, 20).

GENE	PROTEIN	DISTRIBUTION	LOCALIZATION	TIMING
scn1a	$Na_v1.1$	Neurons (mainly GABAergic interneuron and motorneuron), Glial cells	Soma, Dendrites, Proximal AIS	Increased expression in post-natal weeke III. Decreased expression after the postnatal month I
scn2a	$Na_v1.2$	Neurons	Proximal AIS	Increased expression in post-natal week III
scn3a	$Na_v1.3$	Neurons	Soma, Dendrites, Axon	Embryonic and neonatal stages
scn5a		Neurons	Axon	Adulthood
scn8a	$Na_v1.6$	Neurons, Glial cells, Schwann cells	Soma, Dendrites, Distal AIS, Ranvier nodes	Increased expression after birth- It is the predominant form expressed in adulthood

***Table 1*. VGSC alpha subunits expression in the CNS**. VGSCs expression, localization and timing of expression is strictly regulated during CNS development and in adulthood (21-27).

Regulation of VGSCs

The regulation of the activity of VGSCs occurs primarily at the transcriptional level where several alternative splicing sites allow the expression of different isoforms. For example, the alternative splicing of the scn1a gene, with the inclusion of the exon 5N, instead of the 5A, determines the synthesis of a channel with a more rapid recovery from the inactivation state (28). Another example is the scn8a gene, where only the presence of Fox-1 transcription factor determines the inclusion of the 18A exon that leads to the synthesis of the functional protein (29). β1b subunit is a cytosolic soluble protein that derivers from an alternative splicing of the scn1b gene during the development of the CNS where it is involved in neurite outgrowth (30) and regulation of Na_V 1.2 and Na_V 1.3 channel proprieties (8).

Secondly, a role of pivotal importance in the control of VGSCs is due to post-translational modifications that regulate their insertion into the plasma membrane, the stability of the channel and its functionality (31, 32) and references therein. The most important post-translational modification is the extensive glycosylation of the extracellular loop between the S5 and S6 segment in the I and II domain that plays an important role in modulating the opening of the channel as a function of the membrane voltage. On the other hand, the intracellular loops between the I and II domain have phosphorylation sites, target of, among several kinases, both the Protein Kinase A (PKA), that determines a reduction of the ion flux in channel, and Protein kinase C (PKC) that causes a reduction of the ion flux in the channel and a slower speed of inactivation (33, 34).

VGSCs subunits expression in mammals CNS

The most expressed alpha subunits in mammals CNS (Na_V 1.1, Na_V 1.2, Na_V 1.3, Na_V 1.5, Na_V 1.6) are distributed in clusters in different neuronal compartments (Table 1). The process of subcellular localization of different isoforms, in particular at the axon initial segment (AIS) and Ranvier nodes (31, 35, 36) is fundamental, as they perform different functions in the initiation and back-propagation of the action potential. The Na_V 1.2 subunit, which has a high activation threshold, is more present in the proximal region of the initial segment of the axon, where it performs the main function of back-propagation, while the Na_V 1.6, which has a low activation threshold, is more expressed in the distal portion of the initial segment of the axon, functional to the propagation of the action potential (28). Since the α-subunits are able to diffuse freely in the plasma membrane, their aggregation in

different regions of the membrane is mediated by the binding with specific proteins associated with cytoskeleton, as well as with glial cell proteins, which, for instance, regulate their localization at the level of Ranvier nodes (31, 35, 37).

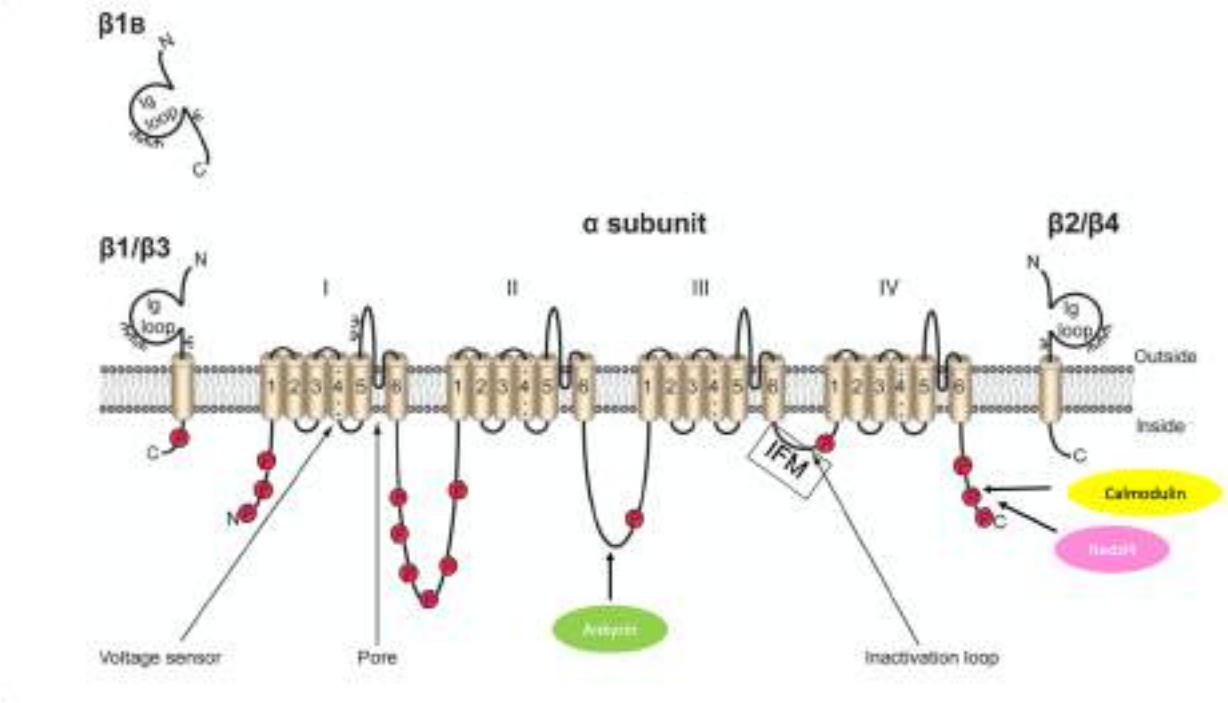

Figure 1. **Topology of VGSC alpha and beta subunits.** Representation of VGSCs alpha and beta subunits. The voltage sensor, the pore and inactivation loop (with IFM motif) are indicated by arrow. Red circles represent some phosphorylation sites (10, 32) while ψ represent glycosylation ones. Some VGSCs interactors are reported in color circles (28). Figure modified by (7).

VGSCs role in neuronal differentiation

Numerous studies on mouse animal models have pointed out that alterations in channel expression, localization, and function, together with related sodium currents defects, cause impairment in neuronal excitability that correlate, in some cases, with impaired neuronal differentiation. Indeed, β1 expression ad localization to the plasma membrane is necessary to neurite outgrowth both *in vitro* and *in vivo* models (19, 20, 38). Also β1b expression is reported to be important during neuron development, regulating neurite elongation (30). Moreover, a functional correlation between $Na_V1.6$ and β1 expression and neurite outgrowth during CNS development has been described, indeed β1 dependent neuritogenesis required the localization of $Na_V1.6$ to the AIS and its high frequency firing (39). In addition, also $Na_V1.9$ (expressed in the peripheral nervous system) is localized in mammalian axons

and growth cones, therefore, suppression of Na_V 1.9 subunit expression reduced axon elongation in $Na_V 1.9^{-/-}$ mice (40).

Other studies conducted in zebrafish animal model have emphasized the key role of VGSCs in neuronal differentiation. In particular, the fundamental role of Na_V1.6 in the development of the correct neural network was assessed thanks to the generation of a Na_V 1.6 knockdown zebrafish that highlighted altered axonal morphologies of motorneurons, together with delayed axonal outgrowth (41). Moreover, defects in motor axon length, in number of axon branches and in the clustering of synaptic vesicles and maturation of neuromuscular junctions has been pointed out in the Sod1G93R zebrafish (42). This model recapitulates a familiar form of Amyotrophic lateral sclerosis (ALS) pathogenetic phenotype, showing precocious alterations in the regular development of the motor nerve circuitry, and suggest that these alterations are prompted by motor neuron hyperexcitability triggered by anomalies in the I_{NaP} (43).

Amyotrophic lateral sclerosis

Amyotrophic Lateral Sclerosis is a progressive neurodegenerative disease characterized by the degeneration of the cortical, bulbar and spinal motor neurons that leads to neuromuscular system failure and cause the death of the patient in 2-5 years from the diagnosis. ALS is the third most common neurodegenerative disease and the most common motor neuron ones with a mean incidence of 2.8/100,000 and a mean prevalence of 5.40/100,000 in Europe (44). In most cases, the onset of the disease occurs in late adulthood, between 55 and 65 years old individuals, however juvenile (before 25 year) and “young onset” (before 45 year) forms of the disease, represent ~1% and ~10% of all ALS cases (45).

ALS clinical phenotypes

Clinical phenotypes of ALS can be classified based on the level and anatomical area of motor neuron involvement and pattern of onset. Typical ALS involves degeneration of both upper and lower motorneurons. The onset of the disease consists of weakness, cramps, muscle fasciculations, myoclonus and difficulty in performing automatic movements and

usually begins in one of the three main regions of the body (face, arm and leg), although it rarely begins in muscles controlling the trunk and / or breathing. ALS histopathological signs consist of atrophy of the motor cortex and pyramidal tracts, in which scar and sclerotic tissue can be found. Thinning of ventral roots of the spinal cord, a widespread spinal gliosis, neuromuscular junction alterations and skeletal muscle atrophy are also characteristic of the disease (46).

The 90% of ALS cases are sporadic (sALS) with an unknown etiology whereas the 10% of the cases present a positive familial history (fALS) (47). The first disease-causing gene, pinpointed in 1993, is the one encoding the superoxide dismutase 1 (SOD1) enzyme, thanks to the identification of a dominant missense mutations within the gene (see below) (48).

A landmark event in the understanding of ALS pathogenesis was the discovery of mutations in TAR DNA-binding protein 43 (TARDBP) gene, which encodes for TAR DNA-binding protein 43 (TDP-43) protein whose C-terminus is involved in ribonucleoprotein binding and splicing. The mutations in the TARDBP gene, accounting for 4% of familial ALS cases and a smaller percentage of sALS, have highlighted the central role of TDP-43 in ALS pathogenesis and consequently the importance of RNA processing in the pathogenesis of the disease (49). Additional support for this hypothesis came from the discovery of the involvement of Fused in Sarcoma (FUS), another RNA-binding protein involved in ALS pathogenesis. Although missense mutations of FUS gene accounts for a small percentage of fALS (~4%), its discovery represented a landmark in ALS research because of the function homology of this protein with TDP-43 (50). Furthermore, FUS mutations cluster in the RNA-binding domain at the C- terminus of the protein, as seen with TARDBP. These observations strengthened the role of abnormal RNA metabolism in motor neuron degeneration (51). Missense mutations in UBQLN2 gene, coding for Ubiquilin-2, located on the short arm of chromosome X, have been identified as causative of ALS. Mutated Ubiquilin-2, which regulates ubiquitin-mediated protein degradation, may be an important component of the common pathway mediating motorneuron degeneration (47). Other mutations were identified in the chromosome 9 open reading frame 72 (C9orf72) gene, located on the short arm of chromosome 9 and characterized by a GGGGCC hexanucleotide repeat. In a healthy individual, the GGGGCC expansion can range from 2 to 30 repeats, but in patients with C9orf72-associated ALS, it ranges from several hundred to thousands of repeats. Noteworthy, this pathogenic expansion accounts for a remarkable 40% of fALS and

7% of sALS (52). Also, VAPB gene, coding for the vesicle-associated membrane protein associated protein B (VAPB) protein, is a causative gene of a rare autosomal dominant form of ALS, called ALS8 (see below) (53). Other, less frequent, mutations have been identified in genes encoding proteins involved in the maintenance of the cytoskeletal structure (PFN1), autophagy (SQSTM1) and alteration of vesicular transport (OPTN) (47). Moreover, since 2014, seven novel genes associated with ALS MATR3, CHCHD10, TBK1, TUBA4A, NEK1, C21orf2, and CCNF have been identified (54).

SOD1

SOD1 gene, located in the long arm of chromosome 21, encodes the enzyme superoxide dismutase 1 (SOD1), a 32 KDa homodimeric protein with a β-barrel conformation. This ubiquitously expressed enzyme, catalyzes the reduction of reactive oxygen species (ROS) in which superoxide (O_2^-) is transformed into oxygen (O^2) and peroxide (H_2O_2) (55). The main involvement of SOD1 in the pathogenesis of ALS is through mitochondrial disfunction, however other cellular pathways (i.e. proteasome inhibition, toxic extracellular vesicle formation, ER stress) are influenced by mutant SOD1 expression not only in motoneuron in a non-cell autonomous pathogenetic mechanism of the disease (56). Moreover, recent evidence also reports a role of SOD1 as a transcription factor, regulator of cellular metabolism and stabilizer of some RNAs, in response to oxidative stress (57). The frequency of mutations in the SOD1 gene varies from 12% to 23% in patients with fALS and upto 7% in sALS (58). Among these, the D90A (substitution of an aspartic acid in position 90 with an alanine residue) is the most frequent in the European population and causes the disease through an autosomal dominant mechanism (58, 59). The A4V (substitution of the fourth amino acid alanine with valine), instead, is the most frequent mutation in the population of North America, it is an autosomal dominant mutation and determines a very aggressive variant of the disease (58). The G93A substitution (substitution of glycine in position 93 with alanine) was the first to be identified and is the most studied. Since this enzyme is highly expressed in neurons, the first pathogenetic mechanism proposed to explain the selective degeneration of motorneurons was linked to a loss-of-function of the enzyme (60). Numerous evidence, however, revealed that most mutations in the gene, as the G93A itself, did not result in a loss of the enzyme's scavenger function, consequently the more recent hypotheses pointed to the acquisition of new toxic functions of the mutated form of SOD1 (58). Several cytotoxic effects of the mutated form of SOD1 have been hypothesized, such as the formation of protein aggregates, its localization in ectopic sites and the acquisition of

a prion-like behavior, which would determine the acquisition of the mutated phenotype also by wild-type protein (61).

VAPB

The VAPB gene, located in the long arm of chromosome 20, encodes the VAPB protein, an integral membrane protein of the endoplasmic reticulum (ER), member of a conserved vesiscle associated membrane protein associated protein (VAP) family of proteins. This protein has 65% sequence homology with VAPA, with whom it shares the primary structure. The N-terminal part of the protein contains a major sperm protein (MSP) motif flanked by a coiled-coil motif and the transmembrane domain. The MSP domain binds to a variety of proteins from various intracellular compartments and is involved in many cellular processes, such as inter-organelle contact sites formation, lipids transport between organelles, maintenance of calcium homeostasis, unfolded protein response (UPR), organization of the cytoskeleton, autophagy and neurite extension (62, 63). The substitution of the conserved proline residue at position 56 with a serine residue (P56S) in the MSP domain of the protein has been associated to the pathogenesis of a rare, slowly progress form of fALS (53), whose inheritance is autosomal dominant. As shown by previous works, P56S-VAPB forms insoluble cytoplasmic inclusions which cause ER- organelle tethering, mitochondrial toxicity, UPR, imbalance and alterations in endolysosomal pathways with a gain of function mechanism (64, 65). Moreover, P56S-VAPB transgenic mice expressing the mutant protein in all neurons showed signs of ER stress and increased autophagic responses (66, 67). In addition to the toxic gain of function, P56S-VAPB has been shown to induce a further effect by incorporating in the aggregates also wt-VAPB in a dominant negative fashion, thus a loss of function pathogenetic mechanism can occur (68-70). Recently, P56S-VAPB inclusions are reported to be rapidly degraded by the proteasome (71) suggesting that an haploinsufficiency pathogenetic mechanism can be involved in the pathogenesis of ALS8 (72, 73). Consistent with these data, VAPB knockdown in zebrafish led to an impaired motor phenotype with swimming deficits (70). All these studies suggest a VAPB involvement in many functions that are crucial for neuronal survival and ALS pathogenesis.

ALS pathogenetic mechanisms

The studies carried out on cellular and animals model of ALS have allowed to identify pathogenetic mechanisms involving the onset and progression of the disease that not only

involve motorneuron degeneration, but also other cell (i.e astrocytes (74), microglia (75); muscle fibers (61)) in a non-cell autonomous scenario (56). The two most accredited hypotheses to explain motor neuron impairment, probably complementary, imply either the occurrence of a dying forward phenomenon, in which neuron degeneration starts from the upper motor neurons and then extends towards the lower motor neurons, or a retrograde dying back degeneration mechanism, where the first cellular damage occurs at the level of the synaptic terminal of the lower motor neurons and then progress toward the neuron soma in the spinal cord and to the CNS (76) and reference therein. The heterogeneity of the functions of the genes identified as the cause of the familial cases of the disease have contributed to broaden the range of hypotheses about the pathophysiological mechanisms at the bases of the onset and progression of ALS: glutamate excitotoxicity, excessive oxidative stress, mitochondrial damage, formation of toxic aggregates, defects in the cytoskeleton and in the dynamics of axonal transport, defects in RNA metabolism and impaired neuronal excitability (77, 78).

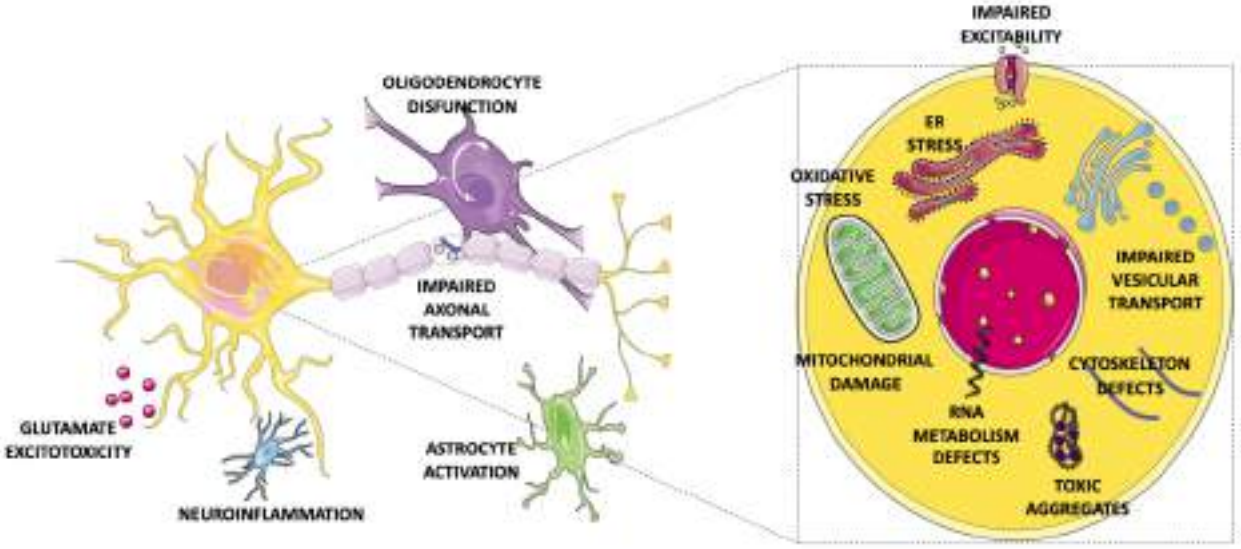

Figure 2. **ALS pathogenetic mechanisms.** Schematic overview of the more studied pathogenetic mechanism of ALS (77). Motorneuron are reported in yellow, oligodendrocyte in purple, microglia in ble and astrocyte in green. Several cellular function are dysregulated during ALS onset and progression in an non-cell autonomous mechanism.

Neuronal excitability as a mechanism of ALS pathogenesis

Neuronal intrinsic excitability can be defined as the capability of the neuron to undergo depolarization in response to a stimulus that exceed a define threshold. This specific

property of the neuron depends on several factors, such as different expression, regulation and intracellular trafficking of receptors and ion channels that regulate the response to the depolarizing input or the alteration of the balance between excitatory and inhibitory inputs causing a lower (hypoexcitability) or higher (hyperexcitability) frequency of depolarization (79). Alteration of neuronal excitability are involved in several detrimental and invalidating diseases (i.e. epilepsy (80), Alzheimer's disease (81)) among which the ALS (82-85). The role of neuronal excitability in ALS onset and progression is highly controversial but more and more evidence suggests a crucial involvement of cellular excitability alterations (both hypo- and hyper-excitability) in different stages of the pathogenesis of the disease (reviewed in (86)). The difficulty in matching and merging the plethora of data reported in literature, due to the fact that these results were obtained in different cellular and animal models, time intervals and motorneurons derived or differentiated from different sources, results in the impossibility to establish an unified mechanism with a temporal definition. Furthermore, it is not clear whether these alterations participate in the pathogenesis, if they are the result of adaptive mechanisms and if they are limited to motorneurons, or shared with other neuronal types, such as inhibitory interneurons, in which structural and electrical alterations have been reported (43, 87). This particular electrical phenotype has aroused interest in the search for alterations in the expression of ion channels involved in the maintenance of intrinsic excitability and in the propagation of the action potential, in particular voltage-dependent sodium channels and voltage-dependent potassium channels. Indeed different studies reveal alterations in VGSCs expression (in particular Na_V 1.1 and Na_V 1.6 subunits) in animal and cellular model of ALS (88-91). Impaired neuronal excitability together with glutamate excitotoxicity represents indeed the targets of one of the few pharmacological treatments that are currently available to improve ALS symptoms by slightly increasing life expectancy in a subset of patients. Indeed, Riluzole (2-amino-trifluoromethoxy benzothiazole), has been the first treatment to be approved by the Food and Drug Administration (FDA) for ALS patients, and it acts on sodium channels determining*, in vitro*, a decrease in the intensity of the current (92-94). *In vivo* studies on *Danio rerio* have identified a decrease in the frequency of spontaneous depolarization in response to treatment with Riluzole in embryos carrying the G93R mutation of SOD1 and whose spinal neurons were characterized by increased frequency of these events (43). Ultimately, the inhibitory activity of Riluzole on the activation of Na_V determines a decrease in glutamate release, with a neuroprotective effect against glutamate excitotoxicity. Some research groups have also proposed an action of Riluzole on potassium voltage dependent and

calcium voltage dependent channels, although the possibility is still debated (94). The effect of Riluzole on patient survival has been evaluated in different studies, and even if initial reports pointed to a significant increase (up to 12-month) in their survival compared to patients treated with the placebo, larger follow-up trials highlighted a decrease in Riluzole therapeutic efficacy between 12 and 21 months of treatment (95).

In vitro and in vivo models of ALS

In vitro and *in vivo* experimental models are still the primary means to investigate the mechanisms underlying the presymptomatic and symptomatic phases of ALS. The first animal model able to recapitulate the human ALS phenotype was the Sod1-G93A mouse, originally reported in 1994. This transgenic mouse develops neurodegeneration of spinal motor neurons and progressive motor deficits leading to paralysis. Since its generation, this model has diverged into a family of strains with different genetic backgrounds and transgene expression levels, that are still broadly used in ALS preclinical research. Subsequently the expression of ALS-related genes in other transgenic organisms has allowed the development of a great variety of invertebrate models, such as Caenorhabditis elegans and Drosophila melanogaster and vertebrate models, such as a variety of rodents, zebrafish, swines and non- human primates reviewed in (96-99).

During my PhD project I took advantage of two different cellular models of ALS.

- G93A NSC34 cell *in vitro* model

Taking advantage of NSC34 cell line, a hybrid cell line often used in the study of motorneuron pathologies, Rizzardini and colleagues generated cell clones that stably express the human form either wt or mutant (G93A) of the SOD1 protein. The first characterization of these clones revealed that SOD1 G93A expression causes no alteration on cell proliferation, but a small decrease in cell viability. Importantly, the authors showed a statistically significant decrease and increase of ROS in SOD1 WT and SOD1 G93A clones respectively (60). Moreover, SOD1 G93A stable clones displayed higher percentage of depolarized mitochondria (60) with alteration in mitochondrial morphology, in terms of high percentage (85%) of fragmented round mitochondria and ultrastructure alterations with defects in mitochondrial cristae. However, no alteration was reported in ER and Golgi structures (100).

- shVAPB NSC34 cell *in vitro* model

The second cellular model that we used is an NSC34 cell line model with a stably expression of a short hairpin (sh) against the VAPB mRNA or a control plasmid (Ctr). This *in vitro* ALS cellular model was established and characterized by Genevini, Colombo and colleagues in 2019 that found an interestingly correlation between VAPB depletion and neurite extension during NSC34 differentiation. Moreover, these defects were associated to increase levels of the Phosphoinositides 4-phosphate (PI4P) in Golgi and vesicular compartments. Interestingly, rescue of VAPB levels in shVAPB clones prevents the defects in neuritogenesis and the increase in PI4P levels. Moreover, cell treatment with inhibitors of PI3Kβ, the kinase responsible for the phosphorylation of PI into PI4P in Golgi compartment, rescue the percentage of shVAPB differentiated cells, suggesting that VAPB depletion affects neuritogenesis through an increase in PI4P levels (73).

Aim of the study

Different studies on Voltage Gated Sodium Channels (VGSCs) have led to the discovery of their involvement in various nervous system pathologies. Mutations in genes coding for the most expressed Na_V isoforms during embryonic development, are associated with defects in neural development and encephalopathies, where at the root of this, there are alterations in the generation of the sodium persistent current and consequently of the intrinsic neuronal excitability (101). Recent studies have also reported that the silencing of Na_V 1.6 subunit causes defects in motoneuron development in a zebrafish model (41) and that its improper localization inhibits neurite elongation in mouse primary motoneuron cultures (39).
Moreover, alteration of persistent sodium current and VGSCs expression, as well as altered neuron morphology, are reported in different model of Amyotrophic Lateral Sclerosis (43, 73, 90, 91).

In this scenario we decided to deeper characterize VGSCs involvement in neurite elongation in health and pathology, taking advantage of the NSC34 *in vitro* model of the disease.

The aim of the project was two fold:

1-To analyse the role of VGSCs expression and activation during NSC34 cells differentiation towards motoneuron-like cells;

2-To characterize VGSCs expression, and neurite extension in two different cellular model of ALS.

Material and Methods

Cell culture and differentiation

NSC34 cell line (supply by Lavinia Cantoni, Università degli Studi di Milano, Milan, Italy) is a hybrid cell line obtained by the fusion of a neuroblastoma with motorneurons derived from mouse spinal cord. This cell line is frequently used to study motorneuron disease because, upon differentiation, can recapitulate a motorneuron-like phenotype (102). Cells were maintained in cultured medium (Dulbecco's modified Eagle medium (DMEM), 1% penicillin/streptomycin, 1% Na^+ pyruvate and 10% Fetal Bovine Serum (FBS)) at 37°C, 5% CO_2 and split every 3-4 days. For differentiation experiments, 24h after seed, culture medium was replaced with differentiation medium (DMEM/F12, 1% Na^+ pyruvate, 1% NEEA, 1% penicillin/streptomycin, 1% FBS and 1μM Retinoic Acid (RA, Sigma-Aldrich, St. Louis, MO)) or culture medium (to obtain undifferentiated controls, UD) for 72h. For differentiation time-course experiments, 24h after seed, culture medium was replaced with culture or differentiation medium. Cell medium was replaced every day for 72h. shVAPB-NSC34 (shVAPB) and Ctr-NSC34 (Ctr) cell line was a kind gift of Dr.Francesca Navone and Prof. Nica Borgese (CNR Institute of Neuroscience, Milan, Italy;(73)). To maintain the selection, stable clones were growth and differentiated in medium added with 250 ug/ml G418 (Gibco/Thermo Fisher Scientific, Waltham, MA). hSOD1wt-NSC34 (SOD1 WT) and hSOD1G93A-NSC34 (SOD1 G93A) cell lines, kindly gift of Dr. Lavinia Cantoni, (Università degli Studi di Milano, Milan, Italy; (60)), were maintained in selection with 500ug/ml G418.
To allow cell adhesion in immunofluorescence and membrane potential detection experiments, glass coverslips were treated with Matrigel (BD Bioscience, Franklin Lakes, NJ) 190 μg / ml for 1.30-2h at 37 °C and then washed twice with PBS.

Tetrodotoxin, Veratridine and PIK93 treatment

Tetrodotoxin (TTX, Hello Bio, Bristol; UK) was dissolved in water and store at -20°C. TTX 1 μM treatment was performed as described in Figure 6. Differentiation medium was replaced every day with or without the addition of TTX 1 μM.

Veratridine (Hello Bio, Bristol; UK) was dissolved in Dimethyl Sulfoxide (DMSO) and store at -20°C. The day after the seed, culture medium was replaced with or without the addition of Veratridine 100 µM and replaced every day for 72h.
PIK93 (Sigma-Aldrich, St. Louis, MO) was resuspended in DMSO and stored at -20°C. The day after differentiation the medium was replaced with differentiation medium containing PIK93 10 nM for another 48 hours.

Plate	Area (mm^2)	Application	UD	24h	48h	72h
Petri	21	WB	$2,7*10^4$	$3,2*10^4$	$4,5*10^4$	$5,3*10^4$
6-well	8	RT-qPCR	10^4	-	-	$2,1*10^4$
6-well	8	IF	$3,3*10^3$	$4,5*10^3$	$6*10^3$	$7,5*10^3$
12-well	3,8	$Disbac_2(3)$	-	-	-	$3,4*10^4$

Table 2. **Number of cells plated in each experiment.** Western Blot analysis (WB). Immunofluorescence experiment (IF). Undifferentiated cells (UD), differentiated cells for 24-48-72 hours of differentiation (24h, 48h, 72h).

Protein extraction and SDS-PAGE immunoblotting

Cells are platelet in petri dish as depicted in Table 2 and differentiate as described above. The day of the experiment, cell medium was discarded and cells are washed with cold (4°C) Phosphate Buffer Saline (PBS, 137 mM NaCl, 2.7 mM KCl , 10 mM Na_2HPO_4, 1.8 mM NaH_2PO_4, pH 7.4) and pellet 10', 800g at 4 °C. Fresh cell pellets were resuspended in PBS plus protease inhibitor 1:1000 (i.p., Sigma-Aldrich, St. Louis, MO) and, after the addition of an equal volume of lysis buffer 2X (40 mM NaCl, 50 mM Tris-HCl pH 7.4, 2 % Triton X-100, 1:1000 i.p) cells were incubated on ice for 10' to allow membranes lysis without the lysis of cell nuclei. The suspension was centrifuged 1000g 4°C for 5' to pellet the nuclei. The protein content of the supernatant was analysed with Bicinconinic Acid (BCA, Euroclone, Pero, Italy) assays. 30 µg of protein were loaded in 7% or 12% polyacrylamide gel and blot onto 22 µm pore nitrocellulose membrane (Merck KGaA, Darmstadt, Germany) at 4°C over night (o.n.) in Transfer Buffer (190 mM glycine, 25 mM Tris-HCl, 620 mM methanol) containing 0,037% SDS. Membrane non-specific binding sites were block in Blocking Buffer (5% non-fat milk powder, 0.1% TWEEN-20 in Tris-Buffered-Saline Buffer; TBS, 20 mM Tris-HCl pH 7.4, 150 mM NaCl) for 12h at 4°C on tilting plate. Membranes were then incubated o.n. at 4°C with primary antibody listed in Table 3 diluted in blocking buffer. To increase the stringency of the analysis and to eliminate the excess o primary antibody three 5-minute wash in blocking

buffer were carried out. Peroxidase-conjugated secondary antibodies (Table 4) diluted in blocking buffer were incubated for 2h at RT on tilting plate. The excess of secondary antibody was then removed with washes in TBS buffer at decreasing concentrations of TWEEN-20 (0.3 %, 0.1 %, absent). Peroxidase activity were revealed using a Western Lightning ultra-chemiluminescent substrate (PerkinElmer Inc., Waltham, MA) and then detected by ChemiDoC XRS + (Bio-Rad Laboratories, Inc, Hercules, CA). Quantification of the intensity of proteins was carried out with Image Lab v. 6.1.

Antibody reactivity and species	Source	Application and dilution
Actin, monoclonal, mouse	Sigma-Aldrich (St Louis, MO), clone AC-74	IB 1:2500
Calnexin, polyclonal, rabbit	Ari Helenius (ETH,Zuerich,CH)	IB 1:6000
GAP43, monoclonal, mouse	Sigma-Aldrich (St Louis, MO)	IB 1:2000
Na,K ATPase		
Na_v 1.6, polyclonal, rabbit	Alomone, Jerusalem, Israel	IF 1:200
Na_vb1, polyclonal, rabbit	Alomone, Jerusalem, Israel	IF 1:200
Sodium-channel (PAN), monoclonal, mouse	Sigma-Aldrich (St Louis, MO), clone K58/35	IB 1:1000
Tubulin, monoclonal, mouse	Sigma-Aldrich (St Louis, MO), clone B-5-1-2	
VAPB	Francesca Navone and Nica Borgese	IB 1:300

Table 3. List of primary antibodies.

RNA extraction and RT-qPCR analysis from NSC34 cell line samples

To analyse the mRNA expression of NSC34 wild-type (wt) cells and mutant clones, cells were plated in 6-well plates (Table 2) and differentiate as described above. After 72h of differentiation, cells were washed in cold PBS and pellet 5', 5000 rpm, 4°C. Cell pellets are then frozen in liquid nitrogen and store at -80°C. RNA was extracted from frozen cell pellets using RNeasy® Mini Kit (Qiagen NV, Hilden, Germany) together with QIAshredder homogenizers (Qiagen NV, Hilden, Germany), following the manufacturer's instructions. To eliminate gDNA contaminations on-column DNase digestion was performed. RNA concentration and purity were measured using the NanoDrop™ One/OneC Microvolume UV-Vis Spectrophotometer (Thermo Fisher Scientific, Waltham, MA). Complementary DNA (cDNA) was obtained using High-Capacity cDNA Reverse Transcription (GeneSpin, Milan, Italy) following the manufacturer's instructions. The qPCR was performed using the 2X Optimum RTL qPCR Master Mix with SYBR® Green (GeneSpin, Milan, Italy) with KiCqStart Primer (M_Actb_1; M_Scn1a_1; M_Scn1b_1; M_Scn2b_1; M_Scn3a_3; M_Scn3b_1;

M_Scn4b_1; M_Scn5a_1; M_Scn8a_3; M_Scn2a1_2, Merck KGaA, Darmstadt, Germany) and carried out in, CFX Connect Real-Time PCR System (Bio-Rad Laboratories, Inc, Hercules, CA). 35 cycles were performed for each reaction: denaturation at 95 °C for 3 minutes, annealing at 52 °C for 25 seconds, elongation at 72 °C for 30 seconds. All reactions were performed in duplicate. CFX Maestro Software was used to collect and analyze data.

Membrane potential detection using the voltage sensitive $DisBaC_2(3)$ probe

The slow-response potential-sensitive probe, Bis-(1,3-Diethyl- thio-barbituric Acid) Trimethine Oxonol ($DisBaC_2(3)$, Thermo Fisher Scientific, Waltham, MA) is an oxonol, a lipophilic anionic molecule that can enter into depolarized cells where it binds to intracellular and membrane proteins and exhibits enhanced fluorescence emission with a red spectral shift. This probe has an excitation maximum of 530 nm and emission maxima of 560 nm. Increased depolarization results in additional influx of the anionic dye and an increase in fluorescence emission. Conversely, hyperpolarization is indicated by a decrease in fluorescence emission. Cells were plated on 12 mm Matrigel treated coverslips in a 12-well plate (Table 2) and differentiated as described above. Membrane potential detection of 72h differentiated cells was performed inside a dark, black, multiwell plates for cell imaging (Euroclone, Pero, Italy). Cells were incubated in VPS-1 (160 mM NaCl, 4,5 M KCl, 2 mM $CaCl_2$, 1 mM $MgCl_2$, 10 mM glucose, 10 mM HEPES pH 7,4) solution containing $DisBaC_2(3)$ 1, 5 or 10 µM for 30' at 37 °C. For the evaluation of membrane potential at basal state the analysis of cell area is necessary to normalize the signal of fluorescence emission to cell confluence. Three images per coverslip (objective 4x) were obtained using Leica DMi1 Inverted Microscope. Area measurement was performed with FiJi and the median area was calculated with Microsoft Excel worksheet. After the acquisition of the basal fluorescence emission with GloMax® Discover Microplate Reader (Promega Corporation, Madison, WI), each well was treated with 150 µl of VSP-2 depolarizing solution (164.5 mM KCl, 2 mM $CaCl_2$, 1 mM $MgCl_2$, 10 mM glucose, 10 mM HEPES pH 7.4) and the fluorescence emission were then measured. Cells fluorescence emission at basal state or after the addition of the depolarizing stimulus was performed with Microsoft Excel worksheet.

Immunofluorescence and confocal microscopy

For immunofluorescence experiments cells were plated on 24mm Matrigel treated coverslips in 6-well plates (Table 2) and differentiate as described above.

$Na_V1.6$ and Na^+/K^+ ATPase immunofluorescence

Cells were fixed with 100% MetOH for 20' at 4°C. MetOH residues were then discarded with two washes in High Salt PBS (HS-PBS; 500 mM NaCl, 20 mM phosphate buffer, pH 7.4). Cells were permeabilize with blocking buffer 1 (BB1, 5% Goat Serum, 5% BSA, 0.3% Triton X-100, PBS 1X) for 30' at RT and then incubated in a humid chamber o.n. 4°C with primary antibody (Table 3) diluted in BB1. The excess of primary antibody was removed with three 5-minutes washes in HS-PBS. Cells were then incubated in a humid dark chamber for 45' with the secondary antibody diluted in BB1 without Triton x-100 (Table 4). The excess of antibody was then removed with three 5-minutes washes in HS-PBS and two 5-minutes washes with low salt concentration (LS-PBS; 150 mM NaCl, 10 mM phosphate buffer pH 7.4).

$Na_V\beta1$ and tubulin immunofluorescence

Cells were fixed in 4 % paraformaldehyde in 4 % sucrose phosphate buffer for 20' at RT. Paraformaldehyde residues were then discarded with two washes in PBS followed by two washes with HS-PBS. Cells were then permeabilize with blocking buffer 2 (BB2, 0.45 M NaCl, 20 mM phosphate buffer, 1: 6 Goat Serum, 0.3 % Triton X-100). Subsequently, cells were incubated. in a humid chamber, with primary antibody (Table 3) diluted in BB2 without Triton X-100 for 2h at RT or o.n 4°C for the detection of $Na_V\beta1$ protein. The excess of primary antibody was then removed with three 5-minutes washes in HS-PBS. Cells were then incubated with the secondary antibody (Table 4) diluted in BB2 without Triton X-100 for 45' at RT. The excess of antibody was then removed with three 5-minutes washes in HS-PBS and two 5-minutes washes with LS-PBS.

For all the experiments nuclei were stained 5' with 4'-6-diamidine-2-phenol (DAPI) diluted in LS-PBS and coverslips were mounted with Mowiol 4-88 on slides.

Reactivity	Conjugation	Source	Application and Dilution
Mouse IgG	Peroxidase	Sigma-Aldrich (St Louis, MO)	IB 1:70000
Mouse IgG	Alexa Fluor 568	Thermo Fisher Scientific (Waltmam, MA)	IF 1:400
Mouse IgG	Alexa Fluor 488	Thermo Fisher Scientific (Waltmam, MA)	IF 1:400
Rabbit IgG	Peroxidase	Sigma-Aldrich (St Louis, MO)	WB 1:12000
Rabbit IgG	Alexa Fluor 568	Thermo Fisher Scientific (Waltmam, MA)	IF 1:400

Table 4. **List of secondary antibodies.**

Image acquisition and analysis

Images were acquired with NIKON ECLIPSE 300 widefield microscope equipped with 20x/0.40 Plan-Apochromat and 60x/1.0 oil Plan-Apochromat objectives with CMOS camera or Zeiss LSM 800 (Carl Zeiss, Oberkochen, Germany) equipped with 10x/0.3 Plan-Neofluar, 40×/1.3 oil Plan-Neofluar and 63x/1.4 oil Plan-Apochromat, objectives and Leica TCS SP5 (Leica microsystem Wetzlar, Germany) equipped with 40×/1.3 oil Plan-Neofluar and 63x/1.4 oil Plan-Apochromat objectives.

For the analysis of neurite length large image were acquire as a sum of adjacent fields.
All images were acquired with the same parameters selecting random fields and taking care to do not reach the saturation of the signal. If images were adjusted in intensity signal, with FiJi (National Institutes of Health, Bethesda, MD), for an easier visualization, identical adjustment was applied.

Statistical analysis

Before data comparison, we checked normal data distribution using Shapiro-Wilk test. To analyse normally distributed data we used Student's *t*-Test for single comparison and one- or two-way ANOVA associated with Turkey's correction. For not-normally distributed data we used Kruskal-Wallis test for multiple comparison, followed by Dunn's correction. For immunoblotting, membrane voltage and RT-qPCR analysis, data were normalized on the control (set as 1) and subsequently subjected to logarithmic transformation. Raw data were collected on a Microsoft Excel spreadsheet and all the statistical analysis were done using GraphPad Prism version 8.0.1. Data are presented as mean ± s.e.m., except for neurite

length, which is presented as median ± interquartile range. P-value are listed on figured as follow: * P<0.05; ** P<0.01; *** P<0.001; **** P<0.0001.

Results

Voltage Gated Sodium Channel expression is regulated during NSC34 cell line differentiation

Given the importance of Voltage Gated Sodium Channels (VGSCs) in neuronal differentiation and Central Nervous System (CNS) development we decided to investigate the correlation between their expression and motorneuron (MN) differentiation. To this aim we took advantage of the NSC34 cell line, an *in vitro* system often used as a model for motoneurons, because, upon differentiation, these cells acquire a motoneuronal phenotype. To perform our study, we applied a previously published protocol (73) able to induce NCS34 differentiation into MN-like cells in 3-6 days upon retinoic acid (RA) treatment in serum deprivation condition.

First, we monitored NSC34 cells differentiation in the first 3 days of the application of the protocol (Figure 3A, B) visualizing cell bodies and neurites by means of immunofluorescence experiments, using an α-Tubulin antibody. During differentiation, cells developed long process and unbranched neurites (Figure 3A). For each experimental time point we measured the longest neurite of 100-200 cells, and we used the measured length to divide cells into four classes: with short (< 50 μm), medium (50 -100 μm), long (100-200 μm), very long (> 200 μm) neurites (Figure 3B, left). As previously reported (73), we selected as the cutoff for differentiation those cells with neurites longer than 100 μm and we evaluated the percentage of differentiated cells for each time point (Figure 3B, middle panel). We observed a sustained increase in the number of differentiated cells at 72h of differentiation (One-way ANOVA test, * $P<0.05$, n=3) and statistically significant differences (Kruskal-Wallis test; **** $P<0.0001$; n=3) in the median length of neurites in each time point of differentiation (Figure 3B, right). Moreover, strikingly, the broader increase in the percentage of differentiated cells occurred in the last 2 days of differentiation, reaching maximum extent in the last 24 hours, as depicted by the slope of the curve (Figure 3B, middle panel).

We then paralleled the morphological characterization of cell differentiation to the amount of VGSCs expressed by cells. The detection of the total pool of VGSCs alpha subunits by

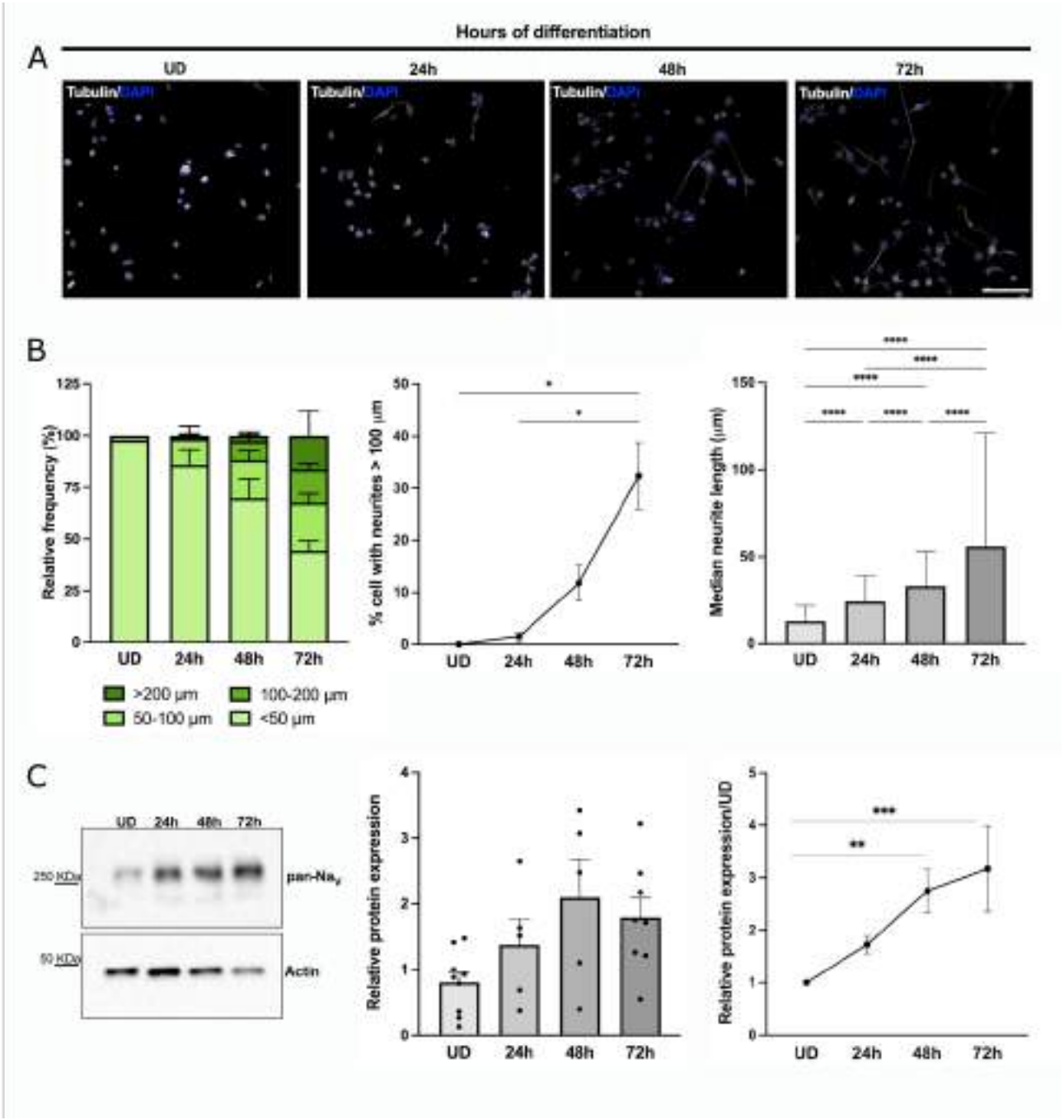

Figure 3. **NSC34 cell differentiation and VGSCs expression. A.** Representative images of immunofluorescence analysis of NSC34 cell differentiation. Cells are labeled with α-tubulin antibody (grey) to analyze neurite length during differentiation; DAPI staining (blue) labeled the nuclei. Scale bar = 130 µm. **B.** Quantification of the longest neurite of 100-300 cells for each time point of each experiment. Cells neurites are divided in 4 classes of length: short (< 50 µm), medium (50 -100 µm), long (100-200 µm), very long (> 200 µm) neurites (left panel). Cells with a neurite longer than 100 µm are considered differentiate (middle panel; Two-way ANOVA; * P<0.05; data on the graph indicate mean value ± s.e.m; n=3). Representation of the medians and interquartile range of the neurites measured for each time point (right panel). Median neurite length increases during differentiation (Kruskal-Wallis test; **** P<0.0001; n=3). **C**. Western blot analysis of VGSCs α-subunit level in protein extracts of undifferentiated (UD) and differentiated cells at different time point of differentiation (24h, 48h, 72h). The α-pan-NaV signal was normalized to the α-actin signal (middle

panel) and subsequently normalized to the UD sample of each experiment (right panel). One-way ANOVA statistical test indicates a statistically significant increase of α-subunits between undifferentiated, and 48h and 72h differentiated cells (*** P<0.001, ** P<0.01; data indicate mean value ± s.e.m; n=8,5,5,8).

means of Western Blot analysis of cell extracts (pan-Na_V antibody, Figure 3C) showed an increase of protein expression during cell differentiation, that is significantly more abundant (One-way ANOVA, ** P<0.01; *** P<0.001) after 48h and 72h of differentiation compared to undifferentiated cells. It is important to note that NSC34 line is an heterogenous cell line and the characteristics of the starting cellular population can slightly vary between experiments and this peculiar aspect of the cell line can at least partially explain why we observed relevant differences in the level of expression of the channels among different experiments (Fig. 3C, middle panel). On top of that, from a technical point of view, the detection of VGSCs alpha subunits is intrinsically difficult due to the size of the molecule and to the binding properties of the antibody that are very sensitive to the experimental conditions that can slightly change in different assays. For these reasons we here reported the data from differentiated cells normalized to the amount of protein from undifferentiated sample of each experiment (Fig. 3C, right panel). Although the statistically significant increase in the protein level was reached after 48 and 72 hours of differentiation, noteworthy the faster increase in VGSCs alpha subunits protein expression occurred within the first 48 hours and particularly in the time window between the 24h-48h of the differentiation, as demonstrated by the curve slope that is steeper in this interval (Figure 3C, right panel).

These observations suggest that in a murine motoneuron-like cell system the differentiation toward the neuronal phenotype, from a morphological point of view, is first preceded and then accompanied by the increased expression of VGSCs alpha subunits.

Since our biochemical analyses only allowed us to evaluate the total pool of VGSCs α-subunits, we took advantage of the RT-qPCR technique to analyse if, during NSC34 cell differentiation, the expression of specific VGSCs α-subunit was more relevant or involved. We considered in our study the five α subunits mostly expressed in the CNS (scn1a, scn2a, scn3a, scn5a, scn8a) and, to complete the molecular characterization of the Na^+ channels playing a role in neuronal differentiation, we also evaluate the mRNAs expression levels of all the 4 VGSCs β-subunits. We noted that only three α (scn1a, scn2a and scn8a) and two β (scn1b and scn3b) VGSCs subunit mRNAs were detectable by RT-qPCR assay in both undifferentiated and fully differentiated NSC34 cell line (Figure 4). Strikingly, the mRNA

levels of all the detectable subunits did not change during differentiation suggesting that the mechanism involved in the increase of VGSCs occurs at the protein level.

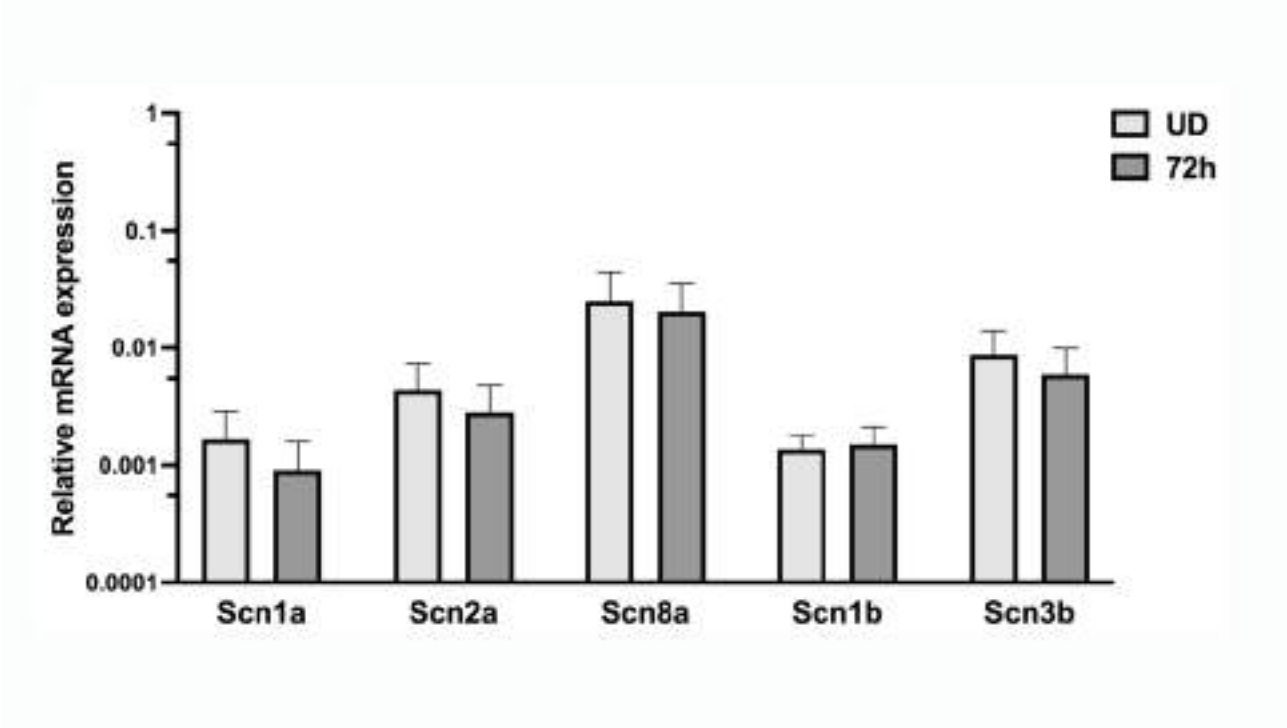

Figure 4. **VGSCs α and β subunits expression in NSC34 cell line.** RT-qPCR mRNA expression levels of Scn1a (Na_V 1.1), Scn2a (Na_V 1.2), Scn8a (Na_V 1.6), Scn1b (β 1), and Scn3b (β 3) in undifferentiated (UD) and differentiated (72h) NSC34 cells. Actin gene is used as the endogenous control to normalize the subunits expression. Data are expressed as mean ± s.e.m of 4 experiments.

Among all the VGSC subunits, Na_V 1.6 and the β1 ones are the better described in the regulation of neurite outgrowth (20, 39). Then, we decide to deeper analyse their localization into cells by means of immunofluorescence experiments on 72h differentiated NSC34. An antibody against Na^+/K^+ ATPase was used to stain plasma membrane and Vesicle associated membrane protein 2 (VAMP2) is used to visualize cell growth cones (Figure 5). Interestingly, both the Na_V 1.6 and β1 proteins localize in differentiated cell growth cones (Figure 5, arrowheads).

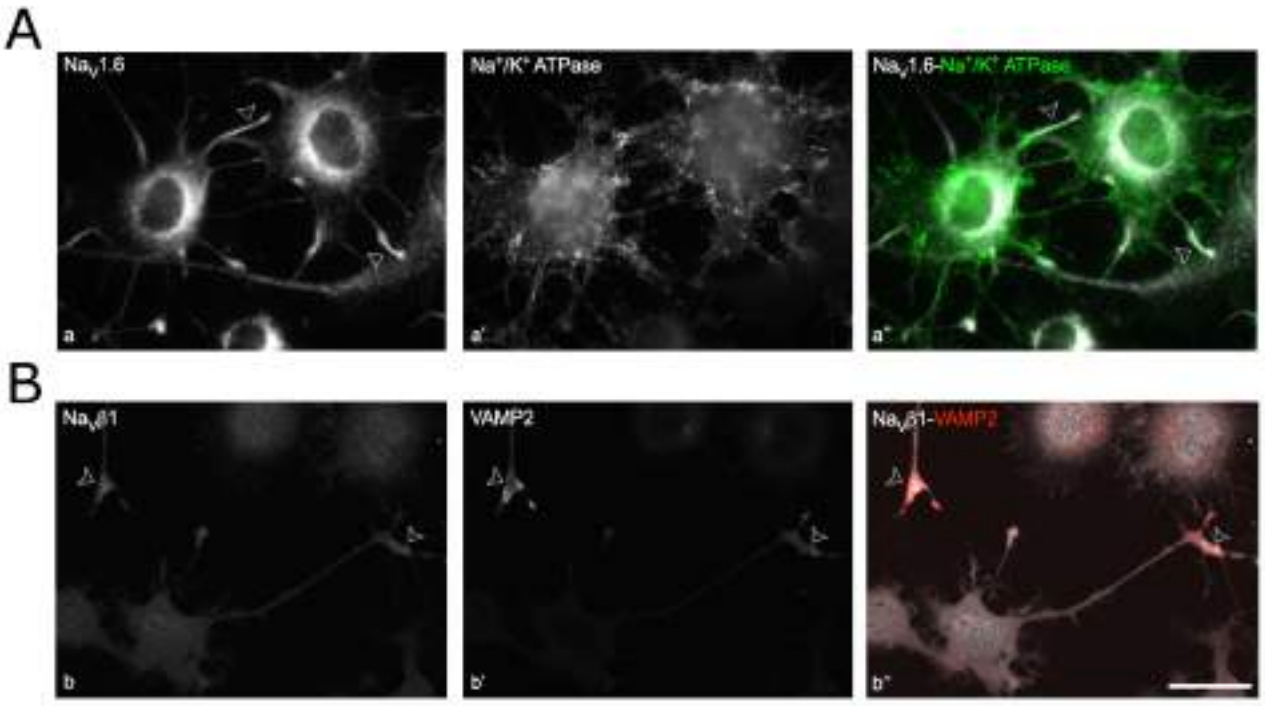

Figure 5. **Analysis of Na_V 1.6 and β1 subunit localization in 72h differentiated NSC34 cells.** **A.** An α–Nav 1.6 (grey) antibody is used to detect Nav 1.6 subunit localization, α– Na^+/K^+ ATPase (green) staining labeled the plasma membrane. Nav 1.6 localizes in cell growth cones (arroweds). **B.** α-Na_V β1 antibody (grey) localizes at cell growth cones (arrowheads). Vesicle associated membrane protein 2 (VAMP2) staining (red) is used to visualize cell growth cones. Scale bar = 50 μm.

Pharmacological modulation of VGSCs impacts on NSC34 cell differentiation

To further dissect the contribution of Na^+ currents through VGSCs to neurite elongation during NSC34 differentiation, we performed a series of pharmacological treatments aimed at increasing or decreasing these currents to look for effects on NSC34 differentiation. We started by blocking Na^+ currents with tetrodotoxin (TTX), treating cells at different time point during the differentiation protocol. One μM TTX is commonly used in electrophysiology experiments to acutely and selectively inhibit the Na^+ currents driven by TTX-sensitive VGSCs (Na_V 1.1, Na_V 1.2, Na_V 1.3, Na_V 1.4, Na_V 1.6, Na_V 1.7). Having verified that 1μM TTX chronic treatment did not interfere with cell viability, we used this concentration to be sure to fully inhibit all TTX-sensitive VGSCs. We treated NSC34 cells at different time points (24 and 48 hours) during the application of the differentiation protocol (as depicted in Figure 6A) and we analysed cells after 72 hours. Once again, we performed immunofluorescence

experiments with α-Tubulin antibody to visualize cell bodies and neurites (Figure 6B) and we quantified cell differentiation measuring the length of the longest neurite of 100-200 cells for each population. Interestingly 1μM TTX treatment affected cell differentiation only when the toxin was administered to cells that were allowed to differentiate for 24 hours and then exposed to the drug for the remaining 48 hours (T24, Figure 6C). In this case, the inhibition of the currents affected, both the percentage of differentiated cells and the median length of the neurites. However, the statistical significance is reached only in the analysis of median length (Figure 6C right panel; Kruskal-Wallis test; ** $P< 0.01$, n=3).

Since the time window from 24 to 48 hours of differentiation seemed to be the crucial one because of the increase in VGSCs protein expression and for neuronal differentiation we wondered if TTX treatment in that specific time frame was sufficient to negatively impact on neurite extension of NSC34 cells. Thus, we performed another experiment treating cells with 1μM TTX only during the T24-T48 interval comparing them with untreated cells and with cell treated from T24 until the end of the differentiation protocol (Figure 6D). Surprisingly, the exposure to the toxin only in T24-48 time interval was sufficient to decrease the percentage of differentiated cells and significantly decreased the median of neurite length (Figure 6D left; Kruskal-Wallis, * $P<0.05$, n=1). Exposure to TTX after 48 hours upon induction of differentiation had no consequences on the final outcome (Figure 6C).

These data confirmed that VGSCs function at the plasma membrane is important to promote neurite extension during neuronal differentiation.

We than wanted to investigate whether increased activity of VGSCs can positively regulate neurite extension, thus we treated NSC34 cells with Veratridine, an alkaloid that binds VGSCs preventing the closure of the channel and increasing membrane depolarization. In electrophysiology experiments Veratridine is often use, acutely, at a concentration of 100 μM to study Veratridine-sensitive VGSC properties. Accordingly, we decide to chronically administer 100 μM Veratridine to NSC34 cells to potentiate Na^+ currents through Veratridine-sensitive VGSCs. Unfortunately, we observed that this treatment profoundly affected cell differentiation capabilities, as shown by an immunofluorescent staining with an α-Tubulin antibody (Figure 7), after 72h of 100 μM Veratridine treatment, cells were completely undifferentiated. Indeed, 100 μM Veratridine treated cells were previously shown to be affected by Ca^{++} and Na^+ overload and this drug is used, *in vitro*, to treat and use cells as a model of excitotoxicity in ALS (103, 104).

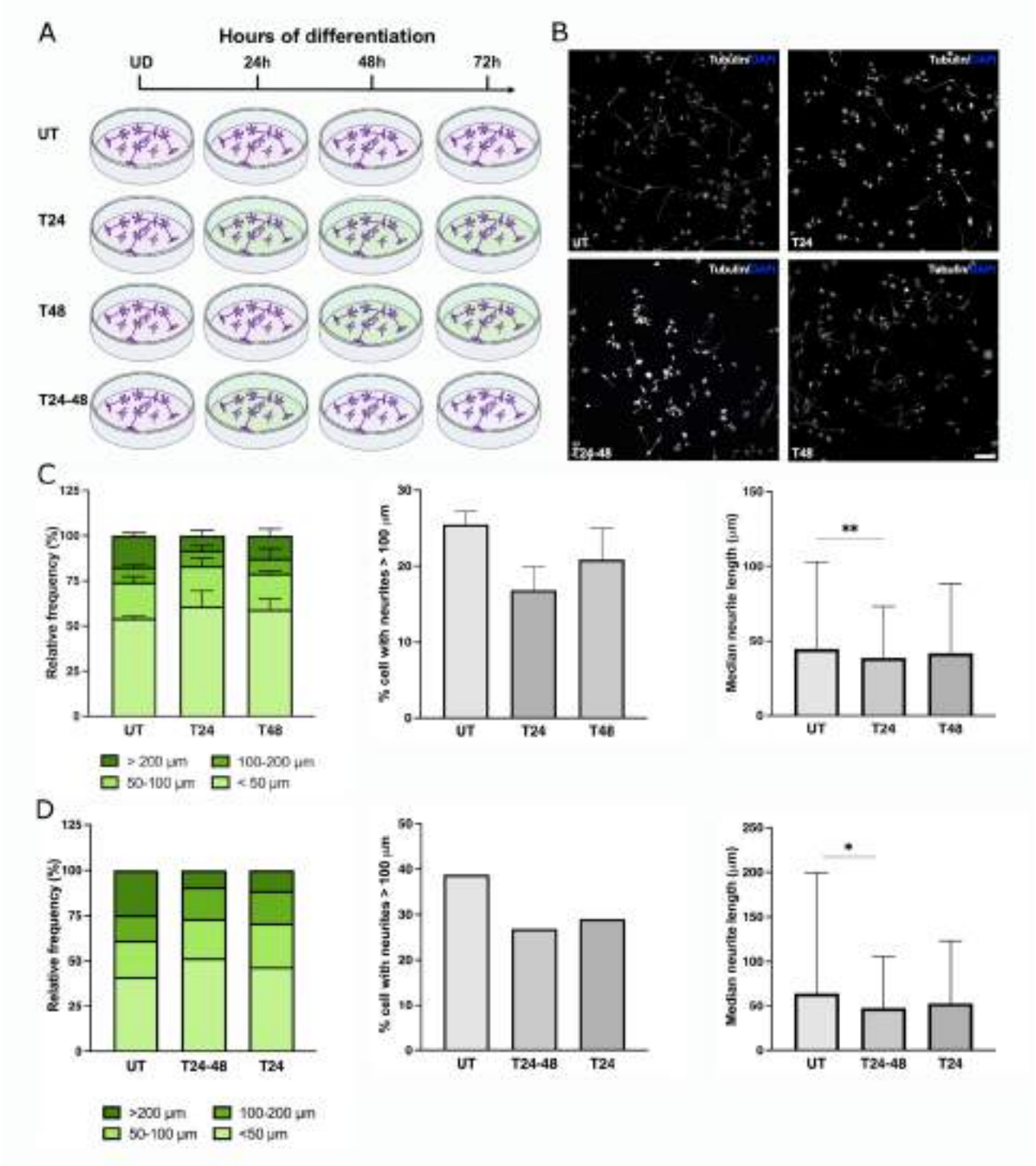

Figure 6. **TTX treatment affects NSC34 cell line differentiation. A.** Schematic representation of TTX 1 µM treatment protocol during NSC34 cell differentiation. UT: untreated cells; T24: cells treated with 1 µM TTX after 24h of differentiation in untreated differentiation medium, for the last 48h of differentiation; T48: cells treated with 1 µM TTX after 48h in untreated differentiation medium for the last 24h; T24-48: cells treated with 1 µM TTX only in the time window between the 24 and the 48 hours of differentiation. **B.** Representative images of immunofluorescent staining with an α-tubulin antibody (grey) to visualize cell bodies and neurites. DAPI staining (blue) labeled the nuclei. Scale

bar = 200 µm. **C.** Quantification of the longest neurite of 100-200 cells for each condition, in each experiment. Cell neurites are divided in 4 classes of length: short (< 50 µm), medium (50 -100 µm), long (100-200 µm), very long (> 200 µm) neurites (right panel). The percentage of differentiated cells (cells with a neurite longer than 100 µm) are reported in the middle graph. Data in left and middle panel are reported as mean ± s.e.m of 3 experiments. Median neurite length is shorter in T24 cells than UT cells (right panel, Kruskal-Wallis test, * P<0.05; data represent medians and interquartile range of the neurite lengths; n=3). **D.** Quantification of 200 cells for each condition. Cell neurites are divided in 4 classes of length: short (< 50 µm), medium (50 -100 µm), long (100-200 µm), very long (> 200 µm) neurites (left panel). The percentage of differentiated cells (cells with a neurite longer than 100 µm) are reported in the center graph (middle panel). T24-48 and T24 differentiated cells are fewer than UT cells. Median neurite length is shorter in T24-48 and T24 cells than UT (right panel, Kruskal-Wallis test; * P<0.05, data represent medians and interquartile range of the neurite lengths n=1).

Pharmacological modulation of VGSCs controls membrane depolarization in differentiated NSC34 cells

VGSCs are involved in the generation and maintenance of membrane potential due to the total charge imbalance, where the intracellular compartment is negatively charged compared to the extracellular one. The use of voltage-sensitive probes allows to carry out measurements simultaneously on cell populations, and in a minimally invasive manner, in order to obtain, in a limited amount of time, measures on a statistically significant base. The $DisBaC_2(3)$ probe is a voltage-sensitive anionic and hydrophobic fluorescent probe, which diffuses into the cell and, when in the cytoplasm, can bind to membrane and cytosolic proteins causing an increase in the emission of fluorescence.

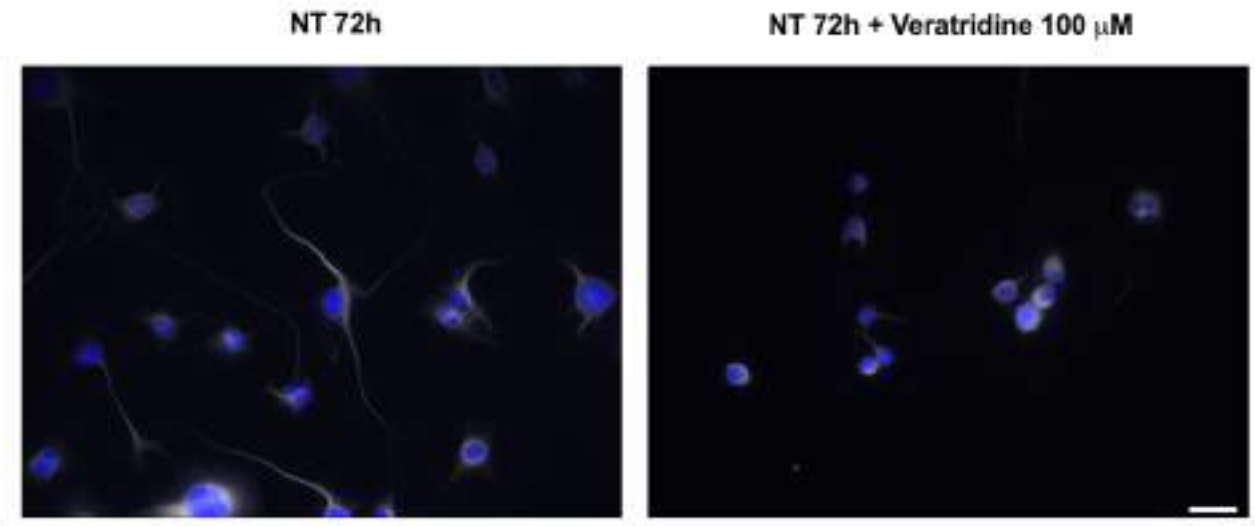

Figure 7. **Veratridine 100 μM treatment affects NSC34 cell differentiation.** Representative images of untreated 72h differentiated cells and 72h differentiated cells treated with 100 μM Veratridine. Cell bodies are visualized thanks to immunofluorescent staining with an α-tubulin antibody (grey). DAPI staining is used to visualize cell nuclei. Scale bar = 50 μM .

As shown in Figure 8A and described in Material and Methods, we incubated differentiated NSC34 cells for 30' with $DisBaC_2(3)$, to allow the diffusion of the probe through the membrane, and then we measured the emission of fluorescence of the cells in basal conditions by exciting the fluorescent probe with a 520nm λ and collecting the emitted photons with a 580-640nm band-pass emission filter. Then, we stimulated cells with 85 mM KCl and measured the fluorescent emission upon depolarization after 1'. As shown in figure 8B, KCl stimulus induced an increase in the emission of fluorescence.

We initially run some preliminary experiments in order to find the right concentration of $DisBaC_2(3)$ allowing us to properly use the probe to analyze the depolarizing status of differentiated NSC34 cells. We observed that increasing concentration of the fluorescent probe resulted in a higher diffusion into the cell and, then, a higher emission of fluorescence in basal conditions (Figure 8C). However, higher concentration of $DisBaC_2(3)$ (10 μM) saturated the system interfering with the possibility to measure further increases in the fluorescence due to depolarization (Figure 8D) while, on the contrary, lower $DisBaC_2(3)$ concentration (1 μM) was always associated with a too high variability in the response to the stimulus (Figure 8D). These observations prompted us to conduct all our functional experiments using a concentration of 5 μM $DisBaC_2(3)$.

Then, we tested if, after 30' of incubation with the probe, the equilibrium is reached and the emitted fluorescent signal was stable or if, conversely, the probe was still able to passively diffuse into the cells and found that, indeed, after 30 minutes incubation with the probe, the system was stable (Figure 8E, left). Similarly, we verified the stability of the signal after 1' following KCl stimulation (Figure 8E, right). The results indicated that the experimental settings were suitable and stable in time allowing us to reliably conduct high-throughput screening experiments.

We treated NSC34 cells with 1 μM TTX and, while no changes in the emitted fluorescence were detectable (data not shown), these can only be seen 1minute after 5 μM TTX treatment suggesting that the sensitivity of the probe in revealing a decrease in the depolarization with

respect to untreated cells is somehow limited (Figure 8F). Conversely, the treatment with 100 µM Veratridine increased NSC34 cells fluorescence emission after the application of the depolarizing stimulus.

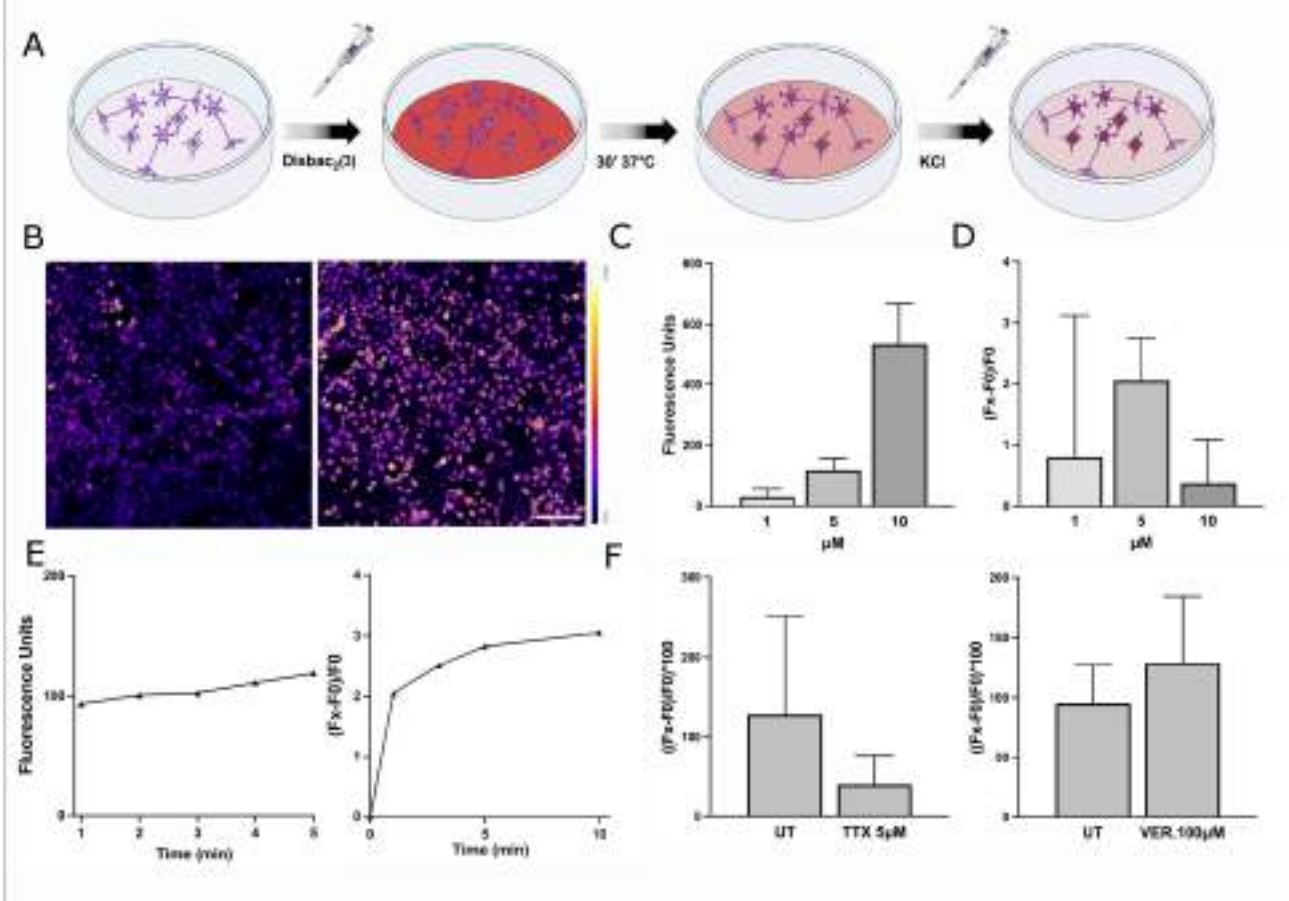

***Figure 8*. Set up of DisBaC$_2$(3) fluorescent probe for 72h differentiated NSC34 cell line membrane potential analysis. A.** Schematic representation of the protocol: 72h differentiated NSC34 cells are incubated 30' with DisBaC$_2$(3) to allow the diffusion of the probe into cells. After the analysis of the basal fluorescent a 85 mM KCl depolarizing stimulus is added to cell media and the fluorescence emission is recorded. **B.** Representative images of cells after 30' of incubation with 5 µM DisBaC$_2$(3) and 1' after the KCl stimulus. Scale bar = 300 µm. **C.** Analysis of the emitted fluorescence units at NSC34 cells basal state after 30' incubation with different concentration (1, 5, 10 µM) DisBaC$_2$(3). **D.** Analysis of the increase in the fluorescence emission 1' after KCl stimulus. **E.** Analysis of 5 µM DisBaC$_2$(3) probe fluorescence emission stability before (left) and after (right) the addition of KCl stimulus to NSC34 cell line. **F.** Analysis of the increase in the fluorescence emission 1' after KCl stimulus in untreated NSC34 cells (UT) or in cell treated with 5 µM TTX 30' before the analysis. **G.** Analysis of the increase in the fluorescence emission 1' after KCl stimulus in untreated NSC34 cells (UT) or in cell treated with 100 µM Veratridine 30' before the analysis. Data are reported as mean value ± s.e.m.; n=3.

Sod1 gene expression affects VGSCs expression and NSC34 differentiation

We have previously demonstrated that zebrafish embryos and NSC34 cells expressing ALS-associated proteins (SOD1 and VAPB, respectively), were characterized by defective axonal or neurite growth and maturation (43, 73). We then examined the differentiation properties of a cellular model of ALS taking advantage of NSC34 cell line stably expressing the human SOD1 wt (SOD1 WT) or G93A mutant (SOD1 G93A) superoxide dismutase enzyme. SOD1 clones, that were previously generated and characterized by Rizzardini, Raimondi and colleagues, displayed mitochondrial alteration in both the functionality and ultrastructure, without any defects in Endoplasmic Reticulum and Golgi Apparatus (60, 100). Once again, we evaluated cell differentiation through the emission of neurites after 72h of treatment with RA, by immunofluorescence staining with α-tubulin antibody (Figure 9A) analysing the number of cells in each of the four classes (<50 μm, 50-100 μm, 100-200 μm,> 200 μm; Figure 9B left) based on the neurite length as previously described.

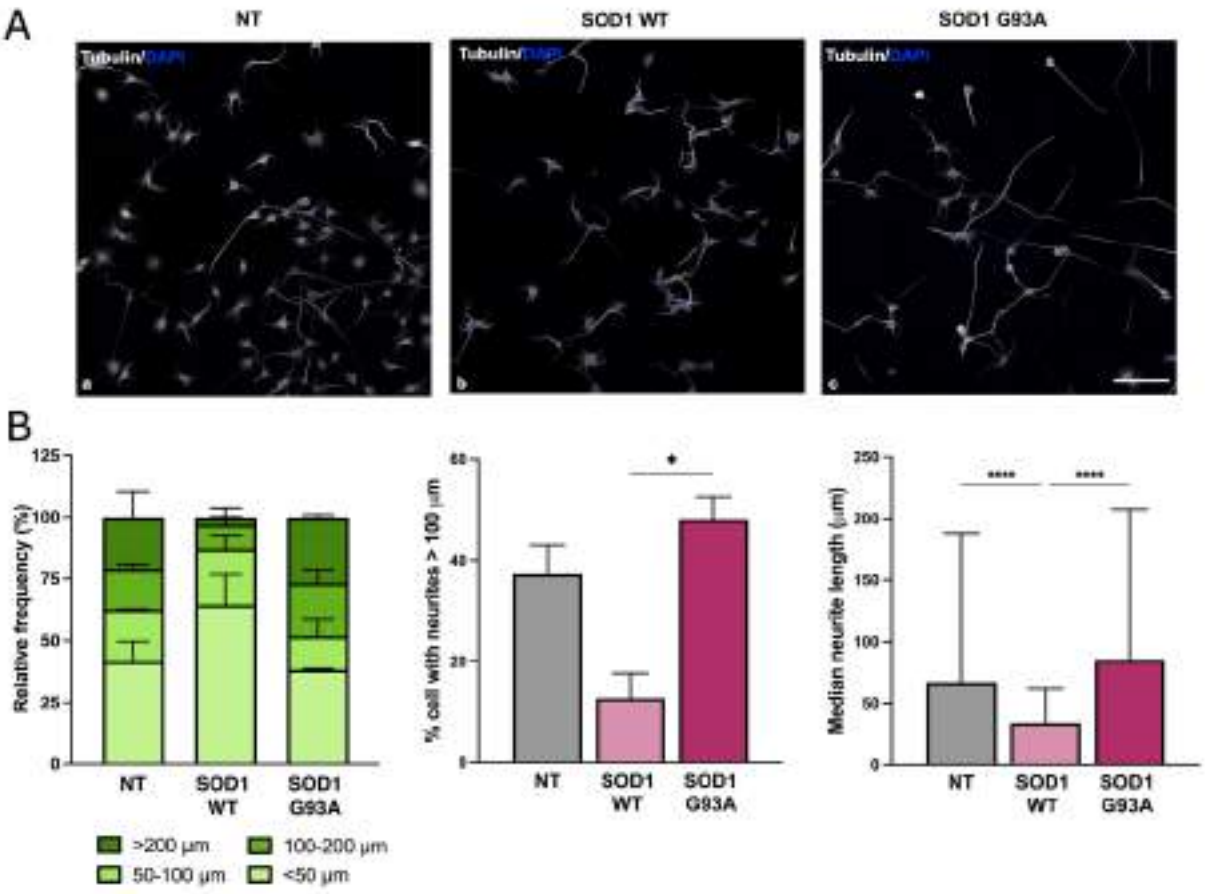

Figure 9. **Analysis of cell differentiation in a SOD1 NSC34 *in vitro* model of ALS. A.** Representative images of immunofluorescence analysis of untrasfected (NT), hSod1 wt (SOD1 WT) and hSod1 G93A (SOD1 G93A) transfected NSC34 cell differentiation. Cells are labeled with α-tubulin antibody (grey) to analyze neurite length during differentiation; DAPI staining (blue) labeled the nuclei. Scale bar = 200 μm. **B.** Quantification of the longest neurite of 250-300 cells for each time point of each experiment. Data are reported as mean ± s.e.m of two experiments. Cell neurites are divided in 4 classes of length: short (< 50 μm), medium (50 -100 μm), long (100-200 μm), very long (> 200 μm) neurites (left panel). Cells with a neurite longer than 100 μm are considered differentiate (middle panel). The percentage of SOD1 WT differentiated cells are lower than NT and SOD1 G93A cells. (One-way ANOVA; *, P<0.05; n=2, central panel). Representation of the medians of the neurites measured for each time point (right panel). Median neurite length is lower in SOD1 wt NSC34 compared to NT and SOD1 G93A cells (Kruskal-Wallis test; **** P<0.0001; n=2).

Unexpectedly, the frequency of cells with longer neurites was clearly lower in cells expressing SOD1 WT than in non-transfected (NT) NSC34 and, in a statistical significant manner, than in SOD1 G93A expressing cells (One-way ANOVA; *, P<0.05; n=2). Moreover, we found a significant decrease in the median length of neurites in SOD1 WT compared to NT (****, P<0.0001) and SOD1 G93A expressing NSC34 (****, P<0.0001) (Figure 9B, right; Kruskal-Wallis test; n=2).

These evidence of impaired neuronal differentiation of NSC34 expressing wt SOD1, at least from the morphological point of view, prompted us to deepen our analyses looking for defects in the protein levels of known markers of differentiation like Growth-Associated Protein 43 (GAP43) and Vesicle-associated membrane protein-associated protein B (VAPB). As can be seen in the representative blots and quantifications (Figure 10), the levels of these two proteins in the three cell populations increased at 72h of differentiation, compared to undifferentiated cells indicating that, indeed, at least from the biochemical point of view, the differentiative process is equally active in the three experimental groups. This apparent discrepancy between the results from the morphological and biochemical analyses is not completely unexpected as we have previously reported a similar phenomenon in another cellular model of ALS, namely NSC34 cells expressing lower level of VAPB protein, where we hypothesized that the defective neurite extension could be due to differentiation proteins mislocalization (73).

Given the importance of VGSCs in neurite extension described above, we analysed their expression levels in SOD1 WT and G93A transfected cells compared to NT. Immunoblot

analyses on undifferentiated and differentiated cell lysates with antibodies recognizing the alpha subunit of VGSCs (pan-Na_V)

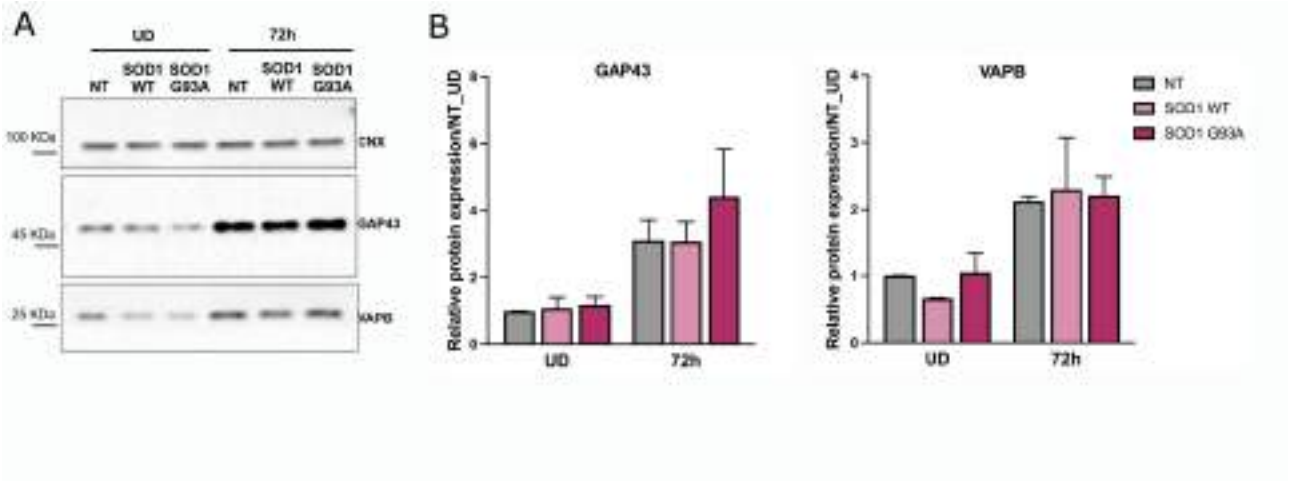

Figure 10. **GAP43 and VAPB expression is not affected during SOD1 WT and G93A NSC34 differentiation. A.** Western blot analysis of Growth-Associated Protein 43 GAP43 and Vesicle-associated membrane protein-associated protein B VAPB protein expression in undifferentiated (UD) and 72h differentiated (72h) untrasfected (NT) hSod1 wt (SOD1 WT) and hSod1 G93A (SOD1 G93A) transfected NSC34 cells. Calnexin (CNX) signal is used as loading control. **B.** Quantification of GAP43 and VAPB signal normalize to CNX and expressed in relation to the undifferentiated NT control (NT_UD) of each experiment. Data are reported as mean ± s.e.m (n=3).

showed a significant reduction in the protein levels in SOD1 WT 72h differentiated cells compared to both the other experimental groups. (Figure 11A; Two-way ANOVA test; * $P<0.05$; ** $P<0.01$; n=3). Interestingly, while these experiments confirmed the increase in the expression levels of VGSCs in NT and SOD1 G93A expressing cells during differentiation, the protein level of the channel in SOD1 WT cells was completely unchanged upon exposure to retinoic acid. For the reasons exposed above, protein quantification from Western Blots were always normalized to the actin signal (as a loading control) and expressed in relation to the undifferentiated NT control cells for each experiment.

Since the immunoblot analysis gives us the information about the total pool of VGSCs α subunits we wondered if a specific α subunit expression is more affected in SOD1 WT cells. To this aim we analysed the mRNA expression of the three α subunits detectable in NSC34 (Figure 11B, C, D). The data, in accordance to the protein ones, show reduced mRNA levels in SOD1 WT cells compared to the other experimental group. Surprisingly, the analysis of the β subunits (Figure 11E, F) show higher level of β1 subunit in SOD1 WT and G93A

expressing cells compared to control NT NSC34 both in undifferentiated and differentiated conditions in a statistically significant manner (Two-way ANOVA; * P<0.05**; P<0.01; n=3). Moreover, scn3b expression is higher in undifferentiated SOD1 G93A NSC34 (Two-way ANOVA; * P<0.05; n=3). Since VGSCs β-subunits are important for channel localization and kinetics regulation (6), more experiments need to be conducted to analyse scn1b protein expression and localization in SOD1 expressing cell.

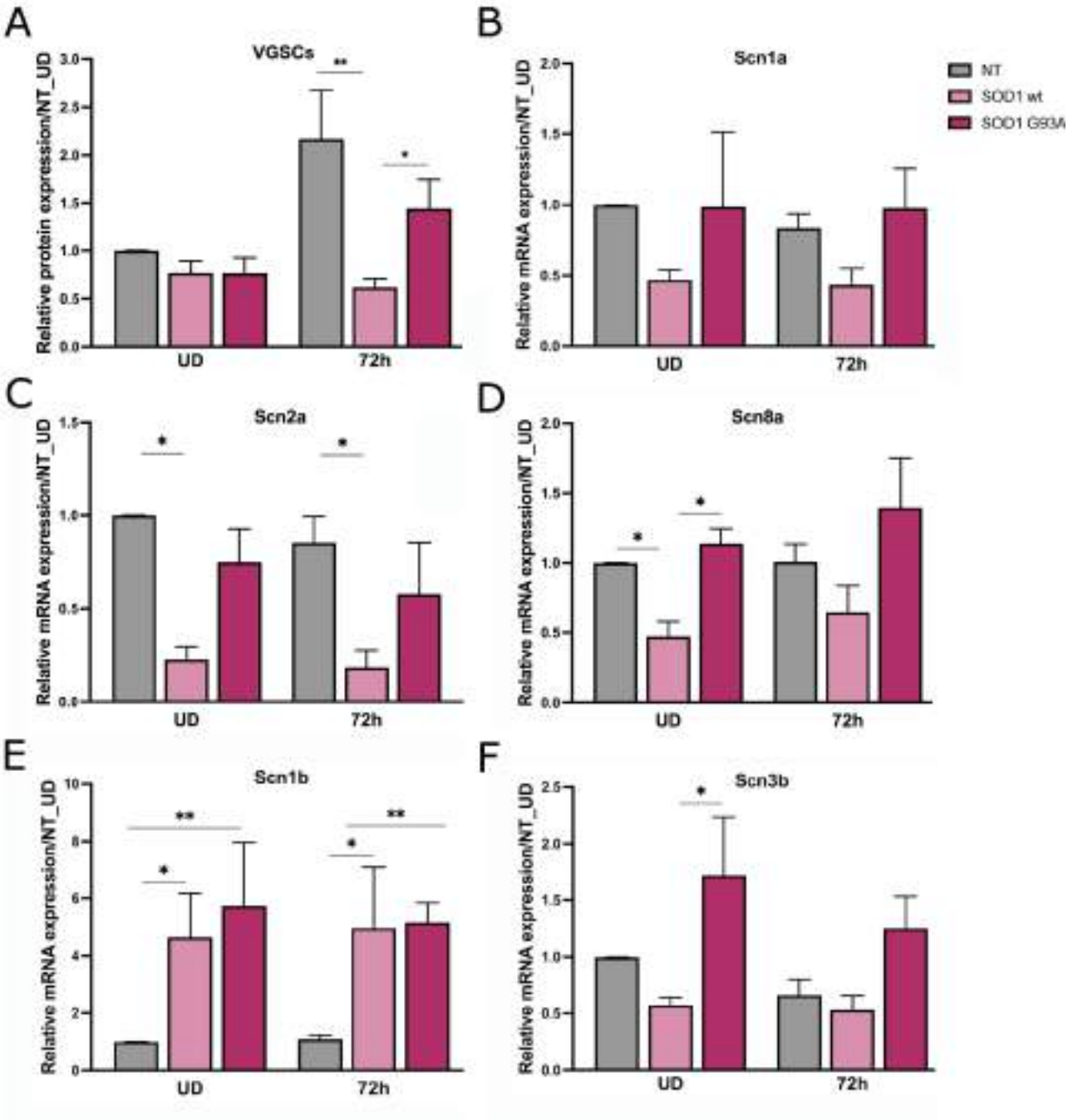

Figure 11. **VGSCs expression in SOD1 WT and SOD1 G93A NSC34 compared to NT cells. A.** Western blot analysis of VGSCs α-subunit level in protein extracts of undifferentiated (UD) and

72h differentiated (72h) untransfected (NT), hSod1 wt (SOD1 WT) and hSod1 G93A (SOD1 G93A) transfected NSC34 cells. The α-pan-NaV signal is normalized to the α-actin signal as loading control and subsequently normalized to the untransfected UD (NT_UD) sample of each experiment. Two-way ANOVA test indicates a statistically significant decrease of α-subunits between 72h SOD1 wt cells compared to the other two genotypes (* P<0.05; ** P<0.01). Data on the graph indicate mean value ± s.e.m of three experiments. **B-F.** RT-qPCR of VGSCs α (scn1a (Na_V 1.1), scn2a (Na_V 1.2), scn8a (Na_V 1.6)) and β (scn1b (β1), scn3b (β3)) subunits mRNA expression in UD and 72h NT, SOD1 wt, SOD1 G93A NSC34. Data are normalized to Actin signal (as control) and expressed in relation to the NT_UD of each experiment. Scn1b subunit expression statistically significant increase in SOD1 WT and G93A NSC34. Data are reported as mean value ± s.e.m. of 3 experiments. (Two-way ANOVA; * P<0.05; ** P<0.01).

Given the greater downregulation of Na_V 1.6 mRNA subunit expression in SOD1 WT cells we decided to analyse the localization of the protein by means of immunofluorescence experiments (Figure12). DAPI staining was used to visualize cell nuclei. As expected, Na_V 1.6 staining is lower in SOD1 WT clones compare to NT cells (Figure 12B) and, moreover, also SOD1 G93A clone presents lower Na_V 1.6 signal. However, the correct Na_V 1.6 localization at the growth cones is lost only in SOD1 WT cells compared to both NT and SOD1 G93A clones (Figure 12, arrowheads).

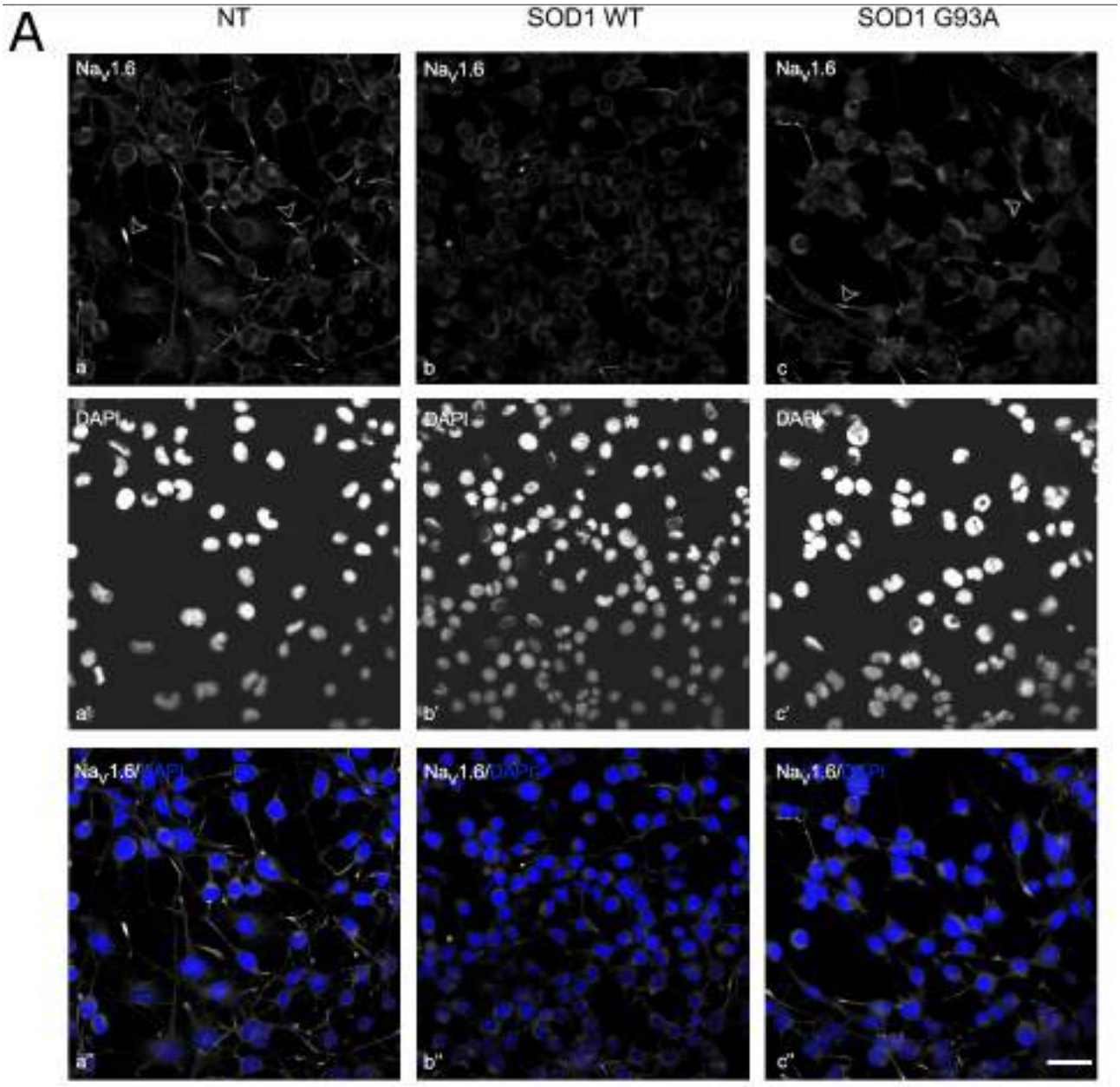
A
NT
SOD1 WT
SOD1 G93A
Na$_v$1.6
DAPI
Na$_v$1.6/DAPI
a
b
c
a'
b'
c'
a''
b''
c''
B
Fluorescence units/ N° cell
3×10^7
2×10^7
1×10^7
0
****
****
*
NT
SOD1 WT
SOD1 G93A

Figure 12. **Analysis of Na_V 1.6 subunit localization in 72h differentiated SOD1 WT and SOD1 G93A NSC34 cells compared to NT NSC34 cells. A.** An α–Nav 1.6 antibody (grey) is used to detect Nav 1.6 subunit localization. DAPI staining (blue) is used to label nuclei. Nav 1.6 subunits localizes in cell growth cones of NT and SOD1 G93A NSC34 (arrowheads). The signal of Nav 1.6 in SOD1 WT cells is lower compared to the other two genotypes and Nav 1.6 does not localizes at the growth cones. Scale bar = 50 μm. **B.** Quantification of Nav 1.6 fluorescent emission signal normalized to the number of cells in each fields. Data are reported as mean ± s.e.m of 10 fields (One-way ANOVA; * P<0.05; **** P<0.0001).

In the end, we decide to analyse if changes in VGSCs expression in SOD1 WT cells are related to changes in cell membrane potential and response to the depolarizing stimulus. Taking advantages of $DisBaC_2(3)$ system, described above, we measured membrane potential at the basal state, normalizing the emitted fluorescent signal to the area occupied by the cells and then, normalized to the NT control (Figure 13A). Then, we analysed the response 1' after the administration of the depolarizing stimulus (Figure 13B). No significant differences were seen in the emitted signals among the three cell populations. However, a small increase was appreciable in the signals emitted in SOD1 WT membrane potential compared to the other two experimental groups.

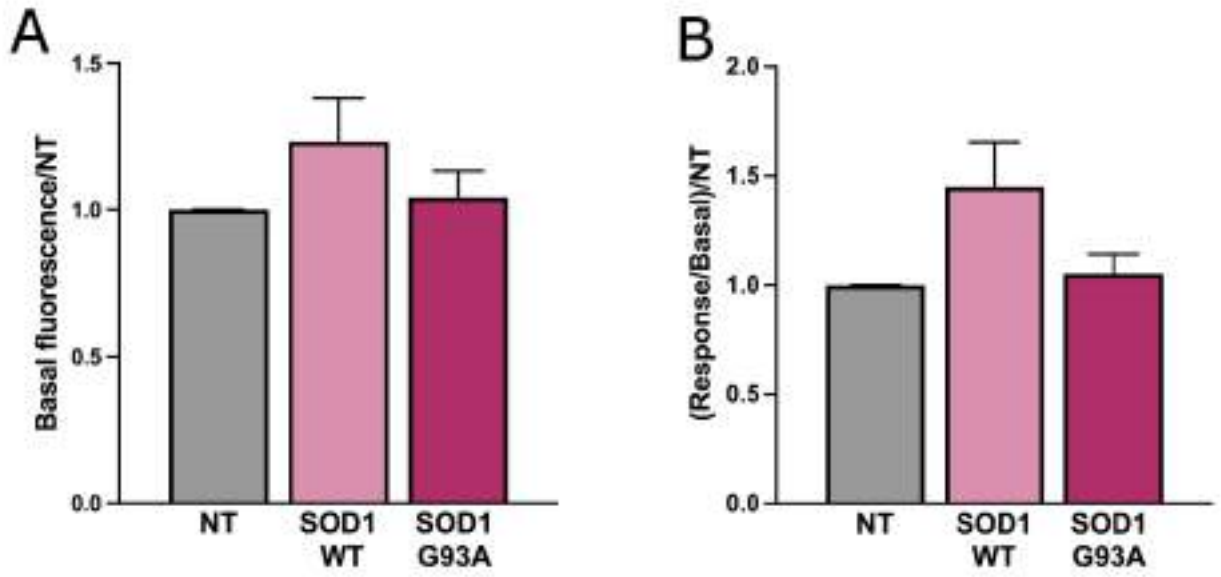

Figure 13. **SOD1 NSC34 membrane potential analysis with $DisBaC_2(3)$ fluorescent probe. A.** Analysis of NSC34 basal fluorescence in untransfected (NT), hSod1 wt (SOD1 WT) and hSod1 G93A (SOD1 G93A) transfected 72h differentiated cells after 30' incubation with 5 μM $DisBaC_2(3)$. Fluorescence units are normalized to the area occupied by the cells on the coverslip and then normalized to the NT control of each experiment. Data are reported as mean value ± s.e.m of three experiments. **B.** NT, SOD1 WT and SOD1 G93A 72h differentiated NSC34 fluorescence emission after 1' of KCl stimulus. Data are reported as ratio between fluorescence emission after and before

the depolarizing stimulus and normalized to the NT control of each experiment. Histograms represent the mean value ± s.e.m of three experiment.

VAPB expression is involved in NSC34 cells membrane potential maintenance

Vesicle-associated-membrane-protein-associated-protein B is a protein expressed in the Endoplasmic Reticulum where is implicated in multiple cellular function such as membrane contact sites formation, lipid transport, HCN channel trafficking (62, 105). Moreover, mutant VAPB protein is one of the genes involved in the pathogenesis of fALS. Recent study (73) suggest that a VAPB haploinsufficiency mechanism can be involved in the onset and pathogenesis of ALS8. In particular, VAPB haploinsufficiency is reported to be involved in neuritogenesis defects and PI4P increased levels in a shVAPB NSC34 ALS *in vitro* model that presents only 10% residual expression of VAPB protein.

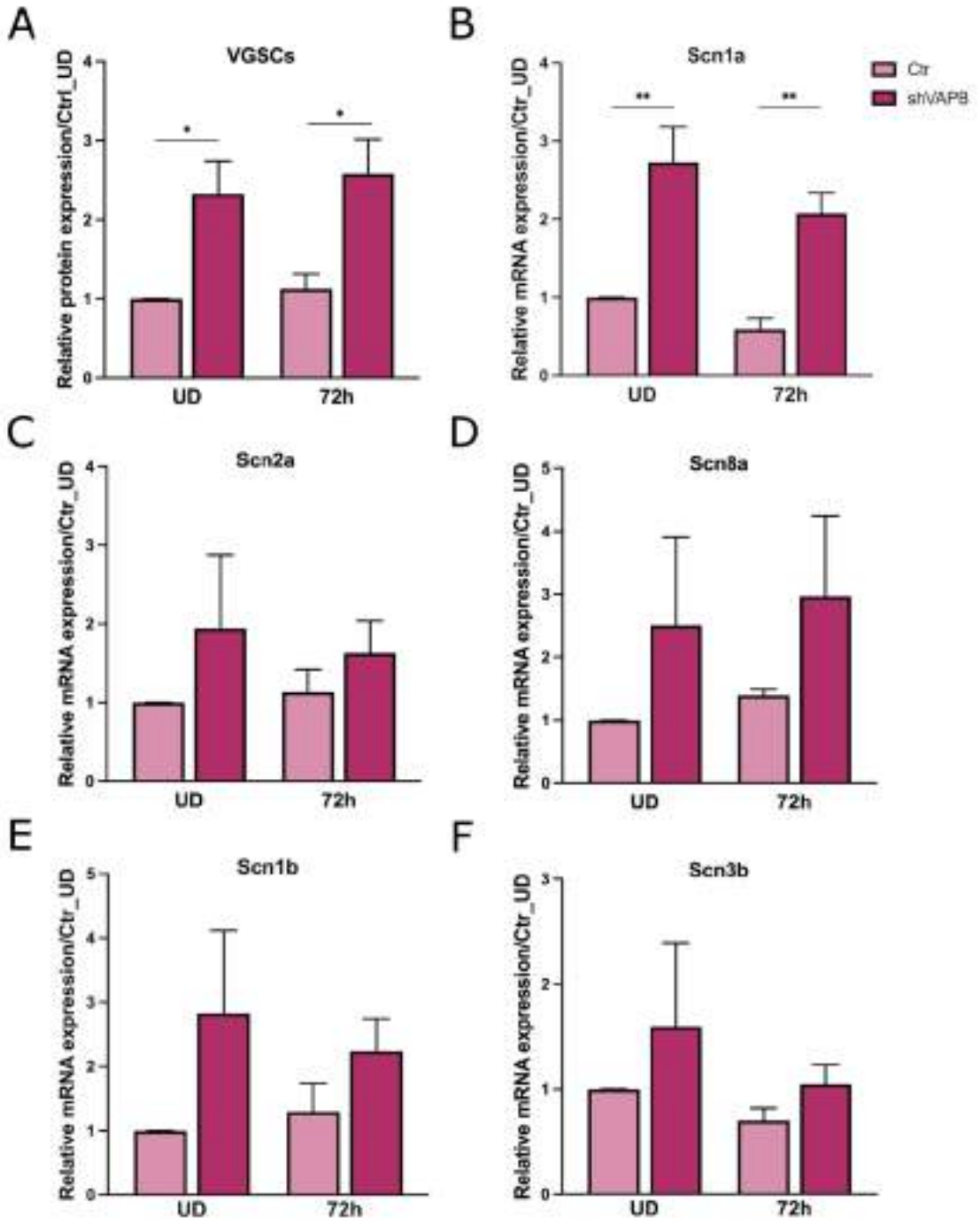

Figure 14. **VGSCs expression analysis in shVAPB NSC34 ALS *in vitro* model of ALS. A.** Western blot analysis of VGSCs α-subunit level in protein extracts of undifferentiated (UD) and 72h differentiated (72h) NSC34 transfected with a short hairpin (sh) against VAPB mRNA (shVAPB) or with a control vector (Ctr) The α-pan-Na_V signal is normalized to the α-actin signal as loading control and subsequently normalized to the UD Ctr (Ctr_UD) sample of each experiment. Two-way ANOVA test indicates a statistically significant increase of α-subunits expression in both UD and 72h shVAPB (* $P<0.05$). Data on the graph indicate mean value ± s.e.m of three experiments. **B-F** RT-qPCR of VGSCs α (scn1a (Na_V 1.1), scn2a (Na_V 1.2), scn8a (Na_V 1.6)) and β (scn1b (β1), scn3b (β3)) subunits mRNA expression in UD and 72h differentiated Ctr and shVAPB NSC34. Data are normalized to Actin signal (as control) and expressed in relation to the Ctr_UD of each experiment. Scn1a subunit

expression statistically significant increase in shVAPB undifferentiated and differentiated NSC34 compared to Ctr. Data are reported as mean value ± s.e.m. of 3 experiments. (Two-way ANOVA; ** P<0.01).

Since during our study we observed a correlation between defective neuritogenesis and VGSCs expression/function, we decided to analyse if VGSCs expression is impaired in shVAPB NSC34 *in vitro* model, compared to Ctr NSC34 cells. However, in contrast to what we observed until now, the expression of the total pool of VGSCs alpha subunits normalized to Actin signal (as loading control) and expressed in relation to the undifferentiated Ctr of each experiment, is statistically significant higher in shVAPB clone respect to Ctr cells (Figure 14A, Two-way ANOVA; *, P<0.05, n=3) both in undifferentiated and differentiated cells. One again we analysed the mRNA expression of the three α and two β subunits detectable in NSC34 (Figure 14B, C, D, E, F). The data, in accordance to the protein ones, show a higher mRNA expression in shVAPB cells compared to Ctr for all the analysed subunits with a statistical significance in scn1a gene expression (Two-way ANOVA; ** P<0.01; n=3).

Then, we analysed the membrane potential of shVAPB cells to evaluate if VAPB insufficiency alters NSC34 capability to depolarize. Despite a small increased in membrane potential at the basal state in shVAPB cells compared to control (expressed as fluorescence units normalize to the area occupied by the cells and then normalized to the Ctr, Figure 15A), shVAPB NSC34 response to the depolarizing stimulus is lower compared to Ctr cells in a statistically significant manner (Figure 15B, t-student test; **, P<0.01, n=7).

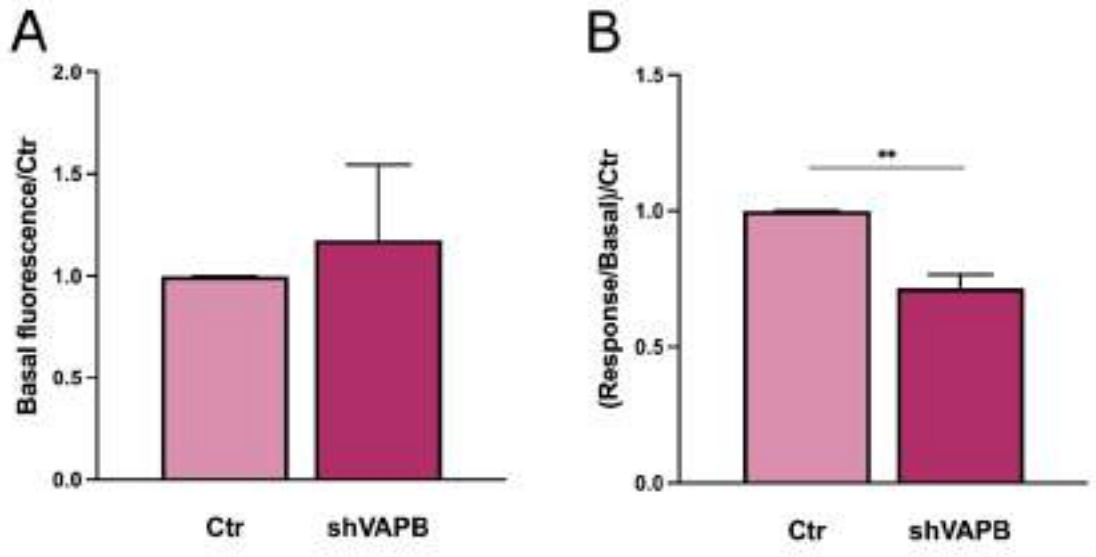

Figure 15. **Membrane potential analysis of shVAPB NSC34. A.** Analysis of NSC34 basal fluorescence in shVAPB and Ctr 72h differentiated cells after 30' incubation with 5 μM $DisBaC_2(3)$. Fluorescence units are normalized to the area occupied by the cells on the coverslip and normalize to the Ctr. Data are reported as mean value ± s.e.m of seven experiments. **B.** shVAPB and Ctr 72h differentiated NSC34 fluorescence emission after 1' of KCl stimulus. Data are reported as ratio between fluorescence emission after and before the depolarizing stimulus and normalized to the ratio of Ctr of each experiment. Histograms represent the mean value ± s.e.m of seven experiments.

To investigate whether shVAPB cells defective depolarization is due to VGSCs mislocalization, we deeper analysed Na_V 1.6 localization in VAPB clones by means of immunofluorescence experiments using an anti-Na_V 1.6 antibody together with an antibody that recognized the Na^+/K^+ ATPase to visualize the plasma membrane (Figure 16). Interestingly, in shVAPB clones Na_V 1.6 staining is not only present in cell growth cones (arrowheads) but in a subpopulation of intracellular vesicles (arrow).

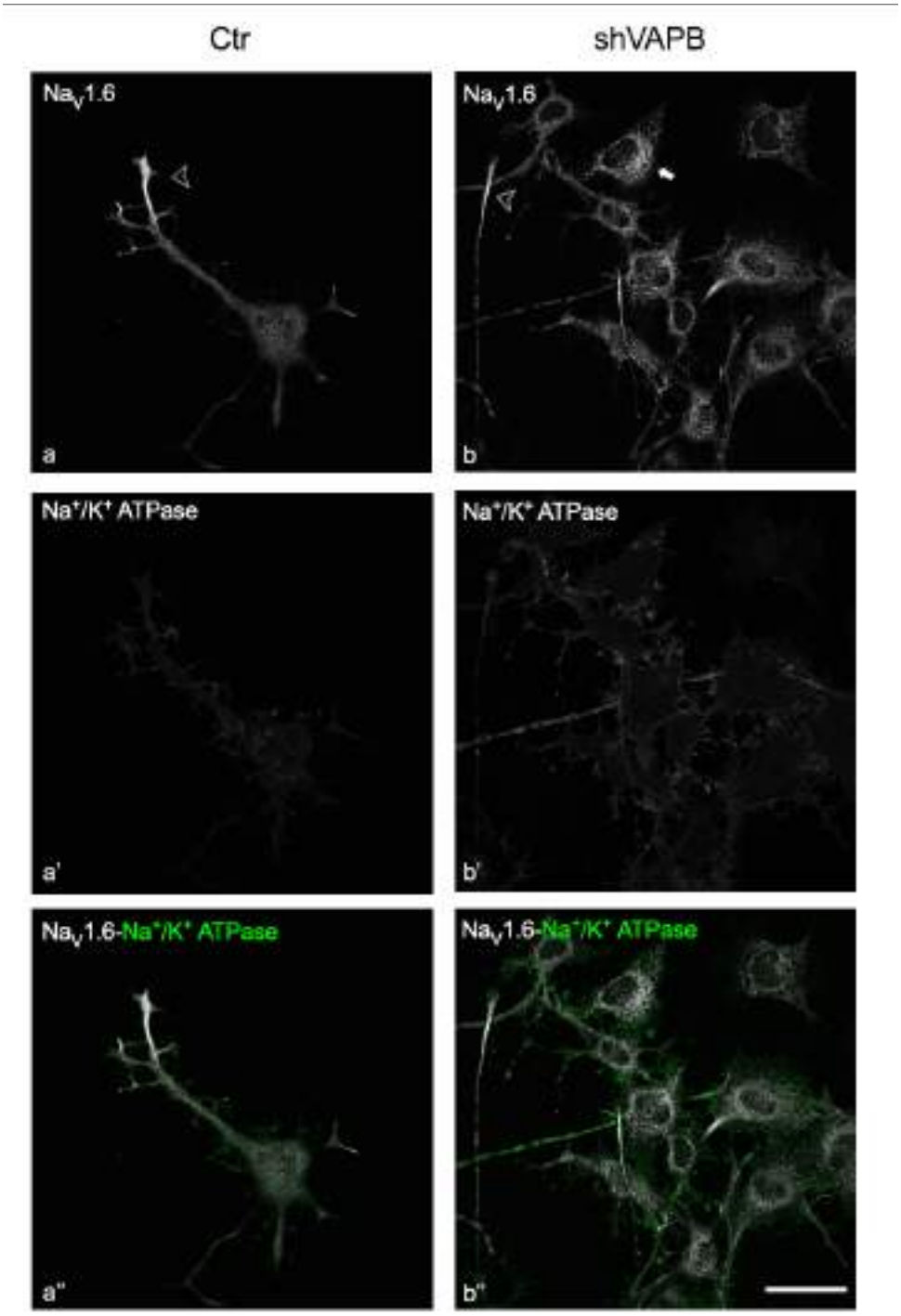

Figure 16. **Analysis of Na$_V$ 1.6 subunit localization in 72h differentiated shVAPB NSC34 compared to Ctr cells.** An α–Nav 1.6 antibody is used to detect Na$_V$ 1.6 subunit localization. , α–Na$^+$/K$^+$ ATPase (green) staining labeled the plasma membrane. Na$_V$ 1.6 subunits localizes in cell growth cones of Ctr and shVAPB NSC34 (arrowheads). However, Nav 1.6 staining of shVAPB cells differs from Ctr because of a intracellular vesicles localization. Scale bar = 50 μm.

Given that the neuritogenesis defects reported in shVAPB NSC34 model are related to PI4P alteration (73) we wondered if shVAPB cells defective depolarization is due to PI4P-

dependent channel mis-localization. To test this hypothesis, we treated shVAPB cells with Pik93, an PI4KIIIβ inhibitor, that at a concentration of 10 nM is reported to rescue NSC34 PI4P level and cell neurites elongation in shVAPB model. The analysis of the response of shVAPB NSC34 to the depolarizing stimulus compared to Ctr cells revealed that Pik93 treatment is able to rescue shVAPB NSC34 capability to depolarize (Figure 17, Two-way ANOVA; *, P<0.05, **, P<0.01, n=3). Surprisingly, Pik93 treatment alters Ctr cells capability to depolarize, suggesting that a PI4P balance is necessary to the correct cell depolarization.

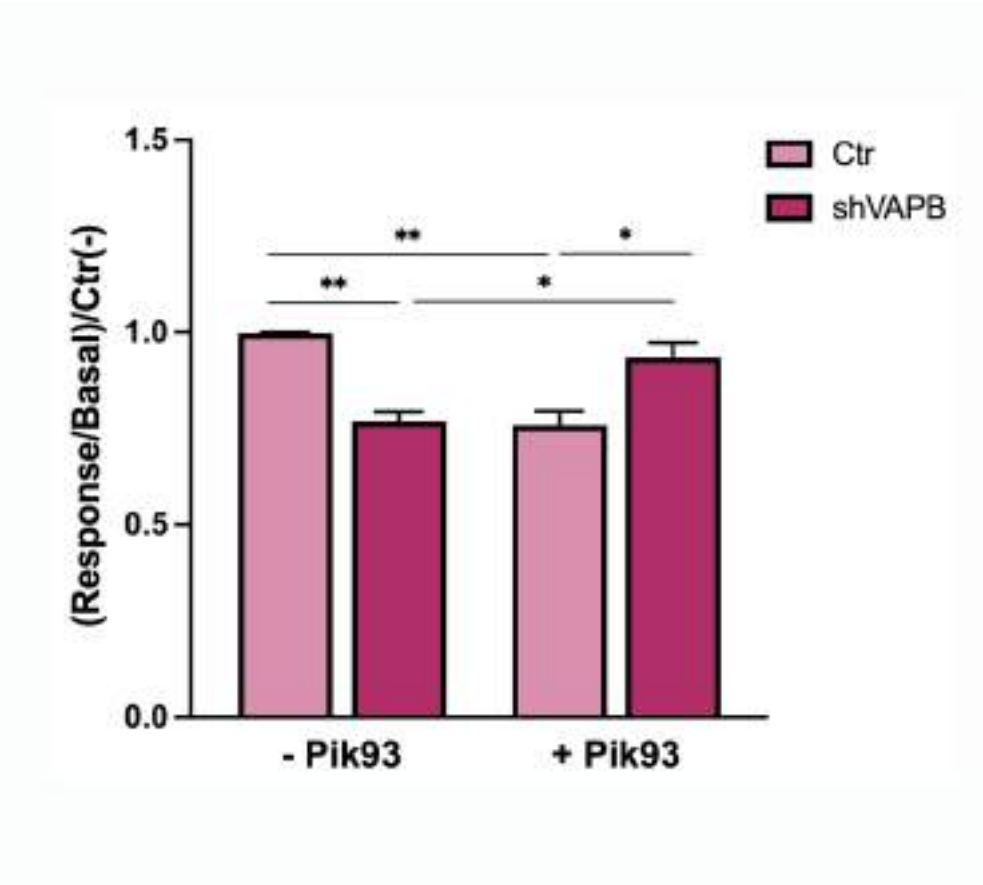

Figure 17. **Analysis of shVAPB NSC34 response to a depolarizing stimulus after Pik93 treatment.** Analysis of the fluorescence emission after 1' of KCl stimulus of shVAPB and Ctr 72h differentiated NSC34 treated (+Pik93) or untreated (-Pik93) with 10nM Pik93, an inhibitor of the PI3Kβ, in the last 48h of differentiation protocol. Data are reported as ratio between fluorescence emission after and before the depolarizing stimulus and normalized to the ratio of the untreated Ctr (Ctr-) of each experiment. Histograms represent the mean value ± s.e.m of three experiments (Two-way ANOVA; * P<0.05; ** P<0.01.

Discussion and Conclusions

Voltage gated sodium channels (VGSCs) are protein complexes made by one alpha and one or two beta subunits and have a role in the generation of Na^+ currents, among which the persistent sodium currents (I_{NaP}). Data in literature point out an involvement of VGSCs and I_{NaP} not only in the regulation of cellular excitability but also in neuron development and neurites outgrowth. Moreover, both VGSCs expression and neurite outgrowth are reported to be dysregulated during Amyotrophic lateral sclerosis pathogenesis both in cellular *in vitro* and animal *in vivo* model of the disease.

In this scenario, the aim of this project was twofold: 1) to find a correlation between Na^+ currents and morphological and functional maturation of motoneurons, 2) to understand if there is a shared mechanism between alteration of Na^+ currents and neurite elongation during the pathogenesis of ALS taking advantage of two different cellular model of ALS.

Voltage gated sodium channel and neurite extension

VGSCs are transmembrane proteins involved in the maintenance of intrinsic neuronal excitability and in the generation and propagation of the action potential in excitable cells. These channels are responsible for the generation of sodium currents, and among these the I_{NaP}. More and more evidence suggest that alteration of VGSCs expression are involved in the regulation of neurite outgrowth. In particular, Na_V 1.6 and β1 subunits localization at the axon initial segment are necessary to the correct neurite outgrowth in mouse neuron primary culture. Moreover, alteration of I_{NaP} and defects in motorneuron axonal outgrowth are reported in a zebrafish model of ALS (39, 43, 106).

For this reason, we decided to investigate the role of VGSCs in motoneuron differentiation taking advantage of the NSC34 murine hybrid cell line, an *in vitro* model often used in the study of motoneuron pathologies as, upon differentiation, these cells acquire several motoneuronal features. Using a previously published differentiation protocol (73) we coupled the analysis of cell morphology with the analysis of VGSCs protein expression showing an increase in VGSCs protein levels during NSC34 differentiation. Our results are in line and

supported by previously published data showing that differentiated NSC34 cells are characterized by an increased density of voltage-dependent Na^+ currents (107) with respect to undifferentiated ones.

We also found the highest increase in the amount of differentiated NSC34 cells in a population between 48 and 72 hours of exposure to the differentiation protocol and interestingly we observed that this increase in differentiation is preceded by an increase in VGSC α subunits protein expression (mostly occurring during the first 48 hours of differentiation). This evidence suggests that the anticipated increase in channel expression might be functional to neuronal differentiation, establishing then a temporal hierarchy regarding the role of VGSCs in this process. On the other hand, the analysis of the mRNA expression levels of the main VGSC α and β subunits expressed in CNS (Na_V 1.1, Na_V 1.2, Na_V 1.3, Na_V 1.5, Na_V 1.6, β1, β2, β3, β4), did not highlight any change in undifferentiated and differentiated cells, thus the mechanisms at the bases of the VGSCs increased expression involve only translation and/or protein stability but which is the specific contribution of these two processes in determining these changes is still a matter of investigation. Indeed, several VGSCs interactors that are involved in regulation of channel localization and stability in the plasma membrane, such as ankyrin, Nedd4, and calmodulin, are proteins involved in and regulated by neuronal maturation and differentiation (13, 108, 109).

To further characterize the relation between VGSCs expression and function and neurite extension in NSC34 cells, we chronically treated the cells with 1μM TTX during the differentiation protocol in order to inhibit the currents mediated by TTX-sensitive VGSCs. Studies conducted *in vitro* and *in vivo* on mouse and zebrafish models already demonstrated a correlation between defects in the persistent sodium current I_{NaP} and altered neurite outgrowth and, indeed, the results of our functional study showed that by inhibiting TTX-sensitive VGSCs in a precise time window (between 24 and 48 hours) during cell differentiation we interfere with neurite extension. This evidence suggests that a fine temporal regulation of VGSCs generated currents is important to modulate neurite outgrowth. A further confirmation of the involvement of VGSCs currents in neurite extensions would be obtained by an inverse approach in which we experimentally increase these currents. To this aim we designed an experiment aiming at the analysis of neurite length upon pharmacological activation of the channels with Veratridine, an alkaloid that by binding the VGSCs alpha subunits prevents the closure of the channel leading to increased currents.

However, to date, we were unable to complete these experiments as the chronic treatment of cells with Veratridine 100 μM, a concentration of the drug used in electrophysiology studies to activate VGSCs, proven to be very unhealthy for our cells, and indeed it was previously shown that the application of this drug to cells for prolonged periods caused a Na^+ and Ca^{++} overload affecting cell viability and morphology possibly through mechanisms linked to excitotoxicity (103, 104). Hence, we are presently looking for another VGSCs activator and in parallel we are trying to establish a Veratridine treatment suitable to chronically activate VGSCs without causing cell toxicity.

Finally, to detect differences in cell membrane depolarization in the entire population of undifferentiated and differentiated NSC34 we used a synthetic voltage-sensitive anionic and hydrophobic fluorescent probe called $DisBaC_2(3)$. This probe is an oxonol, a molecule that diffuses into cell in response to membrane depolarization, and, by binding to membrane and cytosolic proteins within cells it undergoes an increase in its quantum yield and thus increased emission of fluorescence. This peculiar characteristic allows to monitor cell membrane depolarization in a non-invasive high-throughput fashion. Although $DisBaC_2(3)$ has the great advantage to permit the analysis of the membrane depolarization status of an entire cell population, it has the major disadvantage of not being specific for the detection of Na^+ currents, so, by using this probe, it is still impossible to know which are the currents involved in the phenomenon under study. However, the analysis of $DisBaC_2(3)$ emission after acute treatment with either VGSCs inhibitor (TTX) or activator (Veratridine), show that the system is able to detect changes in Na^+ currents.

VGSC and neurite extension in ALS *in vitro* models

In the past 30 years, several different animal models, both vertebrates and invertebrates, were generated and characterize in order to better understand the molecular mechanism that undergoes the onset and progression of ALS (96, 97, 99).

Alterations in VGSCs expression and I_{NaP} dysregulation are reported in several studies on mouse neuron primary culture and motorneuron derived from patient iPSC *in vitro* and also *in vivo* mouse and zebrafish model of ALS (84, 89-91, 110) and, in parallel different ALS cellular and animal models are characterized by changes in neuronal morphology or differentiation properties (43, 73, 110-112). In particular, our previous studies on a zebrafish

G93R model of ALS (42) have shown that already at the earliest developmental stages embryos are characterized by structural motoneurons alterations (i.e. defects in axonal branching) associated to spinal neurons I_{NaP} dependent hyperexcitable phenotype, a phenotype that could be modulated through the administration of Riluzole (43) at a concentration that specifically inhibited the sodium channels at the bases of this pacemaker current. In this model, by restoring the current we reverted the electrical phenotype but also the defects in motor neuron axons outgrowth and development.

Hence, we decided to investigate if VGSCs have a role in the defective neuron maturation and neurite morphology reported in ALS models, taking advantage of two different well characterized NSC34 ALS *in vitro* model systems in which cells were engineered in order to express wt (SOD1 WT) and G93A mutant (SOD1 G93A) human SOD1 enzyme (60, 100) or to lack the expression of VAPB (shVAPB;(73)).

SOD1 G93A NSC34 in vitro model of ALS

The first model we used is the mutant SOD1 NSC34 cell line. Rizzardini, Raimondi and colleagues previously generated and characterized these clones showing that the transfected human form of the SOD1 enzyme is poorly expressed in NSC34 cells compared to the endogenous murine protein. However, despite the small increase of protein expression, the authors reported altered cell viability and defects in mitochondrial morphology, ultrastructure and function in SOD1 G93A clones, suggesting that these defects were due to the expression of the mutant protein and not to an aspecific defect induced by SOD1 overexpression alone (60, 100). Surprisingly, our results showed that SOD1 WT NSC34 cells were more heavily affected when considering the expression of VGSCs α subunits; both the mRNAs and protein levels were significant reduced and this reduction was accompanied by impaired cell differentiation when evaluated through our morphological assay. Strikingly, impaired differentiation was not detectable when examining the expression levels of known markers of differentiation by means of biochemical assays. The defective neurite extension that we observed in SOD1 WT cells was in line with data from the literature showing a small decrease in axonal outgrowth and branching in adult mice motoneurons overexpressing the wt form of the SOD1 enzyme (113). Among the several possible pathways that can be dysregulated upon SOD1 enzyme overexpression, a depletion in reactive oxygen species (ROS) can be involved in neurite extension defects (114). In support of this hypothesis, Rizzardini and colleagues have shown that even if the

increase of the total amount of the SOD1 enzyme due to the transfection of the human wt form of the protein, was quite limited, SOD1 WT clones had lower levels of ROS compared to non-transfected NSC34 and SOD1 G93A clones (60). Conversely, in our hands, SOD1 G93A NSC34 cells could efficiently differentiate into cells with longer neurites with respect to untransfected cells. Our new data on a cellular model of ALS are consistent with the increased neurite branching and outgrowth in adult SOD1 G93A transgenic mice motoneurons compared to non-transgenic littermates as previously reported (113).

While the alfa subunit is responsible of the formation of the pore and the the state of the channel, the beta one is mainly responsible of the regulation of the kinetics of the channel and the interaction with the extracellular environment. Interestingly, the analysis of VGSCs β subunits mRNA expression shows a higher and statistically significant increase in Na_V β1 subunit expression in SOD1 WT and G93A clones both in undifferentiated and differentiated conditions. Indeed, it is important to note that β1 expression is needed to finely tune VGSC protein stability and localization and, together with Na_V 1.6 alpha subunits, in neurons, it is localized in growth cones where it is involved in the process of neurite elongation (39). The immunofluorescence analyses that we performed to localize Na_V 1.6 subunit demonstrated that the lack of Na_V 1.6 expression and localization at the growth cones in SOD1 WT cells.

To investigate if the defects in the expression of VGSCs were associated to altered membrane electric properties we, once again, took advantage of the $DisBaC_2(3)$ probe. Surprisingly, despite the reduced expression of VGSCs, SOD1 WT cells responded to depolarizing stimuli with increased emission of photons from the probe indicating a higher depolarization. The response was higher than that of both untransfected cells and SOD1 G93A expressing clones. Still $DisBaC_2(3)$ is not directly measuring Na^+ currents but it is a probe measuring membrane potential, thus, even though this result can be rather unexpected, it could be due to compensatory or unrelated mechanisms induced by SOD1 WT overexpression and/or the reduction of VGSCs. It has recently been reported, in fact, that in mouse neuron primary culture, a decrease in the activity of the VGSCs causes an increase in the level of the Hyperpolarization-activated cyclic nucleotide-gated channels (HCN) and Ca^+ channels at the plasma membrane. Overall, these events are able to increase the cellular depolarization state (115).

shVAPB NSC34 in vitro model of ALS

The second ALS cellular model we used is represented by NSC34 cells in which the Vesicle-associated membrane protein-associated protein B (VAPB) expression is reduced, presenting only the 10% residual expression of VAPB protein. VAPB is an endoplasmic reticulum (ER) membrane protein involved in several cellular processes such as inter-organelle contact sites formation, non-vesicular lipid transport (116, 117), unfolded protein response (UPR), transport to the plasma membrane, organization of the cytoskeleton, autophagy, phosphoinositides homeostasis and neurite extension. The P56S mutation in the MSP functional domain of the protein is involved in the onset of a rare, late onset, slowly progressive form of ALS (ALS8) that it was firstly characterize in Brazilian patients (53). In early studies about the role of this mutant protein, the presence within cells of mutant VAPB aggregates suggested a pathogenetic mechanism involving the acquisition of a new toxic function in the onset and progression of the disease (65, 68, 71). However, more recent studies showed that P56S-VAPB inclusions were rapidly degraded by the proteasome thus pointing to an haploinsufficiency based mechanism instead. This haploinsufficiency might play a role in the pathogenesis of the disease (71, 72, 118). Other studies on ALS animal models and autoptic samples from ALS patients showed a decrease in VAPB expression (70, 119, 120), highlighting an important role of VAPB haploinsufficiency in the pathogenesis of the disease (62). We and others have previously shown (73, 121) that VAPB-silenced cells are characterized by delays in neuritogenesis and that this delay is linked to a higher intracellular level of Phosphatidylinositol 4-phosphate (PI4P). Indeed, VAPB, together with Oxysterol-binding protein (OSBP) protein, is involved in cholesterol transport and related PI4P contro-transport between the ER and the Golgi apparatus (116). Notably phosphoinositides homeostasis and its localization to certain cellular organelles are fundamental in determining the “identity card” of several organelle membranes involved in multiple cellular functions such as the vesicular transport to the plasma membrane (122). Indeed, decreased level of PI4P are necessary to allow the vesicular transport of vesicles to the periphery that is involve in the delivery of several protein at the plasma membrane, among which ion channels (31, 123).

Therefore, given the defective neurite extension of shVAPB cells (73) we analyse VGSCs expression in silenced NSC34 compared to cells expressing a control vector (Ctr). Surprisingly, although only the mRNA expression of scn1a gene is upregulated in shVAPB clones, the level of VGSC protein α subunits expression was higher in undifferentiated and

differentiated shVAPB cells compared to the controls. However, more analyses of Na_V 1.1 subunit protein expression are needed in order to evaluate if the increase of VGSCs protein levels is only due to Na_V 1.1 protein overexpression or other mechanisms influence the stability of other subunits. Then, we analyzed membrane depolarization of these cells and found a significant reduction in the responsiveness of silenced cells upon administration of a the depolarizing stimulus. This observation is not surprising if we consider that previous studies (105) have shown that VAPB is a strong positive modulator of HCN channels localization at the plasma membrane.

However, since Na_V 1.6 subunit has an important role in neurite outgrowth and neurite extension (39) we analysed if Na_V 1.6 localization could influence shVAPB neuritogenesis and responsiveness to depolarizing stimuli, finding that, in silenced clones, the protein is mis-localized in intracellular vesicular compartment instead of in neurite growth cones. Moreover, Na_V1.6 positive vesicles shape and localization are reminiscent of the PI4P positive puncta we have previously described (73).

Although, PI4P and Na_V1.6 immunofluorescence detection needed the application of specific protocols which differed greatly one from the other, making it impossible to visualize their localization on the same sample, some studies highlighted the important role of PI4P in the regulation of channels localization at the plasma membrane (124). Thus, to investigate the possibility of impaired channel transport to the plasma membrane in our model system, we monitored shVAPB cells responsiveness to depolarizing stimuli after the treatment with PIK93, an inhibitor of PI3Kβ, a kinase responsible of the synthesis of PI4P. We showed, indeed, that inhibition of PI3Kβ was able to rescue both PI4P levels and neuritogenesis in shVAPB clones (73). Interestingly, we were also able to rescue the responsiveness of shVAPB to depolarizing stimuli by treating cells with 10 nM PIK93. These functional assays confirmed the role of PI in channels localization at the plasma membrane.

Furthermore, PIK93 treatment affected also the depolarization response of shCtr cells, revealing that the modulation of PI4P homeostasis was fundamental for excitable cells membrane electrical properties. In support to this hypothesis, Braun and colleagues recently uncovered a relevant role played by PI4P in the regulation of KCNQ1 expression at the plasma membrane in physiological and pathological conditions. In particular, they found a strong correlation between PI4P decreased level at the plasma membrane and decrease KCNQ1 surface localization and its function. These authors proved that these defective

subcellular localization of PI4P and of this K^+ channel had profound implications in the pathogenesis of the Long QT syndrome (125).

Pitfalls and future perspectives

Several different experiments will be performed in future to clarify which are the mechanisms and the pathways involved in the regulation of VGSCs in health and pathologies.

First, to evaluate the amount of VGSCs localized at the plasma membrane, we will identify, by means of biotinylation assays, those receptors that are exposed to the extracellular space and their relative amount with respect to the total amount of the protein expressed by cells. Unfortunately, to date, the assays we performed in this direction gave contrasting results as we encountered two main problems: 1) VGSCs biochemical analysis are difficult to perform because a high amount of protein is necessary for western blot detection and the quality of the transfer and consequently antibody labelling can be quite challenging ; 2) to analyse the expression of VGSCs α subunit that are localize to the plasma membrane over the total pool of VGSCs, distinguish between the biotinylated and non-biotinylated forms, is very difficult because the α subunit is an heavy protein (260KDa) respect to the β one (37KDa). Thus, it is difficult to distinguish between the pool of VGSCs localize al plasma membrane (biotinylated form) over the intracellular pool of VGSCs (non-biotinylated form) that run very close into polyacrylamide gels.

Second, we will perform other immunofluorescence experiments aimed at the evaluation of the colocalization between the channel with known membrane markers to understand which the vesicles population is involved in Na_V transport to the plasma membrane. As for the biochemical approach, also the immune detection of VGSCs in fluorescence experiments is difficult to perform because of their low expression. A possible solution to this problem could be the use of fluorescent toxins (i.e. fluorescent TTX) that with an high binding affinity and specificity will allow the *in vivo* detection of most of VGSC expressed. Moreover, the use of toxins that target a specific VGSCs subunit will allow to identify which are the ones whose expression and distribution might be mainly altered during the pathogenesis of ALS.

Finally, it will be interesting to investigate in depth which are the mechanisms involved in VGSC regulation of neurite extension in physiological and pathological conditions, as several mechanisms and pathways have been hypothesized that can be taken into account:

1) Amyloid precursor protein (APP) expression and phosphorylation is reported to be increase in a SOD1 G93A mouse model of ALS (126). Since phospho-APP interacts with NaV1.6 positively modulating its expression at the plasma membra (Liu 2015), an increase in APP phosphorylation can affects Nav1.6 localization at the plasma membrane during ALS pathogenesis.

2) Calpain is overactivated in hSOD1 G93A mouse model of ALS. Given thar Nav1.6 calpain-dependent proteolysis is associated to an increased persistent sodium current in different cellular and animal model (127-129) (Plantier 2019, Brocard 2015, de la Fuente 2020), it will be interesting to evaluate the activity of calpain in our model of ALS. Moreover, since among all calpain substrates there are some proteins involved in neuron differentiation (i.e. MAP2, neurofilament, spectrin; Chan 1999), a further prospective would be the evaluation of calpain activity during NSC34 differentiation and neuritogenesis in health and disease.

Acknowledgments

I would like to thank Prof.ssa Fancolini that gave me the opportunity to attend her laboratory during the three years of my PhD study encouraging me to be independent.

I would like to acknowledge Prof. Luca Del Giacco, Dr.ssa Ghilardi for they advices.

A special thanks to Dr.ssa Francesca Navone, Prof.ssa Nica Borgese and Dr.ssa Lavinia Cantoni that kindly give me NSC34 wt cells and stable shVAPB and hSOD1 WT and G93A clones.

I am grateful to my colleagues Greta, Lucrezia, Davide that help me a lot during these three years.

A special thanks to Dr.ssa Sara Colombo that support me in facing all the biochemical problem I encountered.

I would like to acknowledge the PhD program in experimental medicine and the Università degli studi di Milano that financially support my Phd.

References

1. Llinás RR. Intrinsic electrical properties of mammalian neurons and CNS function: a historical perspective. Front Cell Neurosci. 2014;8:320.
2. Arendt D. The Evolutionary Assembly of Neuronal Machinery. Curr Biol. 2020;30(10):R603-R16.
3. Stafstrom CE. Persistent sodium current and its role in epilepsy. Epilepsy Curr. 2007;7(1):15-22.
4. Chen-Izu Y, Shaw RM, Pitt GS, Yarov-Yarovoy V, Sack JT, Abriel H, et al. Na+ channel function, regulation, structure, trafficking and sequestration. J Physiol. 2015;593(6):1347-60.
5. Qu Y, Curtis R, Lawson D, Gilbride K, Ge P, DiStefano PS, et al. Differential modulation of sodium channel gating and persistent sodium currents by the beta1, beta2, and beta3 subunits. Mol Cell Neurosci. 2001;18(5):570-80.
6. Bouza AA, Isom LL. Voltage-Gated Sodium Channel β Subunits and Their Related Diseases. Handb Exp Pharmacol. 2018;246:423-50.
7. Brackenbury WJ, Isom LL. Na Channel β Subunits: Overachievers of the Ion Channel Family. Front Pharmacol. 2011;2:53.
8. Kazen-Gillespie KA, Ragsdale DS, D'Andrea MR, Mattei LN, Rogers KE, Isom LL. Cloning, localization, and functional expression of sodium channel beta1A subunits. J Biol Chem. 2000;275(2):1079-88.
9. Isom LL, Ragsdale DS, De Jongh KS, Westenbroek RE, Reber BF, Scheuer T, et al. Structure and function of the beta 2 subunit of brain sodium channels, a transmembrane glycoprotein with a CAM motif. Cell. 1995;83(3):433-42.
10. Catterall WA, Goldin AL, Waxman SG. International Union of Pharmacology. XLVII. Nomenclature and structure-function relationships of voltage-gated sodium channels. Pharmacol Rev. 2005;57(4):397-409.
11. Corry B, Thomas M. Mechanism of ion permeation and selectivity in a voltage gated sodium channel. J Am Chem Soc. 2012;134(3):1840-6.
12. Kruger LC, Isom LL. Voltage-Gated Na+ Channels: Not Just for Conduction. Cold Spring Harb Perspect Biol. 2016;8(6).
13. Savio-Galimberti E, Gollob MH, Darbar D. Voltage-gated sodium channels: biophysics, pharmacology, and related channelopathies. Front Pharmacol. 2012;3:124.

14. Chen C, Calhoun JD, Zhang Y, Lopez-Santiago L, Zhou N, Davis TH, et al. Identification of the cysteine residue responsible for disulfide linkage of Na+ channel α and β2 subunits. J Biol Chem. 2012;287(46):39061-9.
15. O'Malley HA, Isom LL. Sodium channel β subunits: emerging targets in channelopathies. Annu Rev Physiol. 2015;77:481-504.
16. Calhoun JD, Isom LL. The role of non-pore-forming β subunits in physiology and pathophysiology of voltage-gated sodium channels. Handb Exp Pharmacol. 2014;221:51-89.
17. Brackenbury WJ, Isom LL. Voltage-gated Na+ channels: potential for beta subunits as therapeutic targets. Expert Opin Ther Targets. 2008;12(9):1191-203.
18. Patino GA, Isom LL. Electrophysiology and beyond: multiple roles of Na+ channel β subunits in development and disease. Neurosci Lett. 2010;486(2):53-9.
19. Davis TH, Chen C, Isom LL. Sodium channel beta1 subunits promote neurite outgrowth in cerebellar granule neurons. J Biol Chem. 2004;279(49):51424-32.
20. Brackenbury WJ, Davis TH, Chen C, Slat EA, Detrow MJ, Dickendesher TL, et al. Voltage-gated Na+ channel beta1 subunit-mediated neurite outgrowth requires Fyn kinase and contributes to postnatal CNS development in vivo. J Neurosci. 2008;28(12):3246-56.

21. Boiko T, Rasband MN, Levinson SR, Caldwell JH, Mandel G, Trimmer JS, et al. Compact myelin dictates the differential targeting of two sodium channel isoforms in the same axon. Neuron. 2001;30(1):91-104.
22. Goldin AL. Resurgence of sodium channel research. Annu Rev Physiol. 2001;63:871-94.
23. Wu L, Nishiyama K, Hollyfield JG, Wang Q. Localization of Nav1.5 sodium channel protein in the mouse brain. Neuroreport. 2002;13(18):2547-51.
24. Trimmer JS, Rhodes KJ. Localization of voltage-gated ion channels in mammalian brain. Annu Rev Physiol. 2004;66:477-519.
25. Craner MJ, Damarjian TG, Liu S, Hains BC, Lo AC, Black JA, et al. Sodium channels contribute to microglia/macrophage activation and function in EAE and MS. Glia. 2005;49(2):220-9.
26. Tan J, Soderlund DM. Human and rat Nav1.3 voltage-gated sodium channels differ in inactivation properties and sensitivity to the pyrethroid insecticide tefluthrin. Neurotoxicology. 2009;30(1):81-9.

27. Eijkelkamp N, Linley JE, Baker MD, Minett MS, Cregg R, Werdehausen R, et al. Neurological perspectives on voltage-gated sodium channels. Brain. 2012;135(Pt 9):2585-612.
28. Wang J, Ou SW, Wang YJ. Distribution and function of voltage-gated sodium channels in the nervous system. Channels (Austin). 2017;11(6):534-54.
29. O'Brien JE, Drews VL, Jones JM, Dugas JC, Barres BA, Meisler MH. Rbfox proteins regulate alternative splicing of neuronal sodium channel SCN8A. Mol Cell Neurosci. 2012;49(2):120-6.
30. Patino GA, Brackenbury WJ, Bao Y, Lopez-Santiago LF, O'Malley HA, Chen C, et al. Voltage-gated Na+ channel β1B: a secreted cell adhesion molecule involved in human epilepsy. J Neurosci. 2011;31(41):14577-91.
31. Cusdin FS, Clare JJ, Jackson AP. Trafficking and cellular distribution of voltage-gated sodium channels. Traffic. 2008;9(1):17-26.
32. Pei Z, Pan Y, Cummins TR. Posttranslational Modification of Sodium Channels. Handb Exp Pharmacol. 2018;246:101-24.
33. Laedermann CJ, Abriel H, Decosterd I. Post-translational modifications of voltage-gated sodium channels in chronic pain syndromes. Front Pharmacol. 2015;6:263.
34. Onwuli DO, Beltran-Alvarez P. An update on transcriptional and post-translational regulation of brain voltage-gated sodium channels. Amino Acids. 2016;48(3):641-51.
35. Leterrier C, Brachet A, Fache MP, Dargent B. Voltage-gated sodium channel organization in neurons: protein interactions and trafficking pathways. Neurosci Lett. 2010;486(2):92-100.
36. Huang CY, Rasband MN. Axon initial segments: structure, function, and disease. Ann N Y Acad Sci. 2018;1420(1):46-61.
37. Solé L, Tamkun MM. Trafficking mechanisms underlying Na. Channels (Austin). 2020;14(1):1-17.
38. Fein AJ, Wright MA, Slat EA, Ribera AB, Isom LL. scn1bb, a zebrafish ortholog of SCN1B expressed in excitable and nonexcitable cells, affects motor neuron axon morphology and touch sensitivity. J Neurosci. 2008;28(47):12510-22.
39. Brackenbury WJ, Calhoun JD, Chen C, Miyazaki H, Nukina N, Oyama F, et al. Functional reciprocity between Na+ channel Nav1.6 and beta1 subunits in the coordinated regulation of excitability and neurite outgrowth. Proc Natl Acad Sci U S A. 2010;107(5):2283-8.

40. Subramanian N, Wetzel A, Dombert B, Yadav P, Havlicek S, Jablonka S, et al. Role of Na(v)1.9 in activity-dependent axon growth in motoneurons. Hum Mol Genet. 2012;21(16):3655-67.
41. Pineda RH, Svoboda KR, Wright MA, Taylor AD, Novak AE, Gamse JT, et al. Knockdown of Nav1.6a Na+ channels affects zebrafish motoneuron development. Development. 2006;133(19):3827-36.
42. Ramesh T, Lyon AN, Pineda RH, Wang C, Janssen PM, Canan BD, et al. A genetic model of amyotrophic lateral sclerosis in zebrafish displays phenotypic hallmarks of motoneuron disease. Dis Model Mech. 2010;3(9-10):652-62.
43. Benedetti L, Ghilardi A, Rottoli E, De Maglie M, Prosperi L, Perego C, et al. INaP selective inhibition reverts precocious inter- and motorneurons hyperexcitability in the Sod1-G93R zebrafish ALS model. Sci Rep. 2016;6:24515.
44. Chiò A, Logroscino G, Traynor BJ, Collins J, Simeone JC, Goldstein LA, et al. Global epidemiology of amyotrophic lateral sclerosis: a systematic review of the published literature. Neuroepidemiology. 2013;41(2):118-30.
45. Turner MR, Barnwell J, Al-Chalabi A, Eisen A. Young-onset amyotrophic lateral sclerosis: historical and other observations. Brain. 2012;135(Pt 9):2883-91.
46. Hardiman O, Al-Chalabi A, Chio A, Corr EM, Logroscino G, Robberecht W, et al. Amyotrophic lateral sclerosis. Nat Rev Dis Primers. 2017;3:17085.
47. Renton AE, Chiò A, Traynor BJ. State of play in amyotrophic lateral sclerosis genetics. Nat Neurosci. 2014;17(1):17-23.
48. Rosen DR, Siddique T, Patterson D, Figlewicz DA, Sapp P, Hentati A, et al. Mutations in Cu/Zn superoxide dismutase gene are associated with familial amyotrophic lateral sclerosis. Nature. 1993;362(6415):59-62.
49. Prasad A, Bharathi V, Sivalingam V, Girdhar A, Patel BK. Molecular Mechanisms of TDP-43 Misfolding and Pathology in Amyotrophic Lateral Sclerosis. Front Mol Neurosci. 2019;12:25.
50. Blokhuis AM, Groen EJ, Koppers M, van den Berg LH, Pasterkamp RJ. Protein aggregation in amyotrophic lateral sclerosis. Acta Neuropathol. 2013;125(6):777-94.
51. Kwiatkowski TJ, Bosco DA, Leclerc AL, Tamrazian E, Vanderburg CR, Russ C, et al. Mutations in the FUS/TLS gene on chromosome 16 cause familial amyotrophic lateral sclerosis. Science. 2009;323(5918):1205-8.

52. DeJesus-Hernandez M, Mackenzie IR, Boeve BF, Boxer AL, Baker M, Rutherford NJ, et al. Expanded GGGGCC hexanucleotide repeat in noncoding region of C9ORF72 causes chromosome 9p-linked FTD and ALS. Neuron. 2011;72(2):245-56.
53. Nishimura AL, Mitne-Neto M, Silva HC, Richieri-Costa A, Middleton S, Cascio D, et al. A mutation in the vesicle-trafficking protein VAPB causes late-onset spinal muscular atrophy and amyotrophic lateral sclerosis. Am J Hum Genet. 2004;75(5):822-31.
54. Chia R, Chiò A, Traynor BJ. Novel genes associated with amyotrophic lateral sclerosis: diagnostic and clinical implications. Lancet Neurol. 2018;17(1):94-102.
55. Fridovich I. Superoxide radical and superoxide dismutases. Annu Rev Biochem. 1995;64:97-112.
56. Ilieva H, Polymenidou M, Cleveland DW. Non-cell autonomous toxicity in neurodegenerative disorders: ALS and beyond. J Cell Biol. 2009;187(6):761-72.
57. Eleutherio ECA, Silva Magalhães RS, de Araújo Brasil A, Monteiro Neto JR, de Holanda Paranhos L. SOD1, more than just an antioxidant. Arch Biochem Biophys. 2021;697:108701.
58. Kaur SJ, McKeown SR, Rashid S. Mutant SOD1 mediated pathogenesis of Amyotrophic Lateral Sclerosis. Gene. 2016;577(2):109-18.
59. Luigetti M, Conte A, Madia F, Marangi G, Zollino M, Mancuso I, et al. Heterozygous SOD1 D90A mutation presenting as slowly progressive predominant upper motor neuron amyotrophic lateral sclerosis. Neurol Sci. 2009;30(6):517-20.
60. Rizzardini M, Mangolini A, Lupi M, Ubezio P, Bendotti C, Cantoni L. Low levels of ALS-linked Cu/Zn superoxide dismutase increase the production of reactive oxygen species and cause mitochondrial damage and death in motor neuron-like cells. J Neurol Sci. 2005;232(1-2):95-103.
61. Pansarasa O, Bordoni M, Diamanti L, Sproviero D, Gagliardi S, Cereda C. SOD1 in Amyotrophic Lateral Sclerosis: "Ambivalent" Behavior Connected to the Disease. Int J Mol Sci. 2018;19(5).
62. Borgese N, Iacomino N, Colombo SF, Navone F. The Link between VAPB Loss of Function and Amyotrophic Lateral Sclerosis. Cells. 2021;10(8).
63. James C, Kehlenbach RH. The Interactome of the VAP Family of Proteins: An Overview. Cells. 2021;10(7).
64. Kanekura K, Nishimoto I, Aiso S, Matsuoka M. Characterization of amyotrophic lateral sclerosis-linked P56S mutation of vesicle-associated membrane protein-associated protein B (VAPB/ALS8). J Biol Chem. 2006;281(40):30223-33.

65. Fasana E, Fossati M, Ruggiano A, Brambillasca S, Hoogenraad CC, Navone F, et al. A VAPB mutant linked to amyotrophic lateral sclerosis generates a novel form of organized smooth endoplasmic reticulum. FASEB J. 2010;24(5):1419-30.
66. Aliaga L, Lai C, Yu J, Chub N, Shim H, Sun L, et al. Amyotrophic lateral sclerosis-related VAPB P56S mutation differentially affects the function and survival of corticospinal and spinal motor neurons. Hum Mol Genet. 2013;22(21):4293-305.
67. Larroquette F, Seto L, Gaub PL, Kamal B, Wallis D, Larivière R, et al. Vapb/Amyotrophic lateral sclerosis 8 knock-in mice display slowly progressive motor behavior defects accompanying ER stress and autophagic response. Hum Mol Genet. 2015;24(22):6515-29.
68. Teuling E, Ahmed S, Haasdijk E, Demmers J, Steinmetz MO, Akhmanova A, et al. Motor neuron disease-associated mutant vesicle-associated membrane protein-associated protein (VAP) B recruits wild-type VAPs into endoplasmic reticulum-derived tubular aggregates. J Neurosci. 2007;27(36):9801-15.
69. Ratnaparkhi A, Lawless GM, Schweizer FE, Golshani P, Jackson GR. A Drosophila model of ALS: human ALS-associated mutation in VAP33A suggests a dominant negative mechanism. PLoS One. 2008;3(6):e2334.
70. Kabashi E, El Oussini H, Bercier V, Gros-Louis F, Valdmanis PN, McDearmid J, et al. Investigating the contribution of VAPB/ALS8 loss of function in amyotrophic lateral sclerosis. Hum Mol Genet. 2013;22(12):2350-60.
71. Papiani G, Ruggiano A, Fossati M, Raimondi A, Bertoni G, Francolini M, et al. Restructured endoplasmic reticulum generated by mutant amyotrophic lateral sclerosis-linked VAPB is cleared by the proteasome. J Cell Sci. 2012;125(Pt 15):3601-11.
72. Genevini P, Papiani G, Ruggiano A, Cantoni L, Navone F, Borgese N. Amyotrophic lateral sclerosis-linked mutant VAPB inclusions do not interfere with protein degradation pathways or intracellular transport in a cultured cell model. PLoS One. 2014;9(11):e113416.
73. Genevini P, Colombo MN, Venditti R, Marcuzzo S, Colombo SF, Bernasconi P, et al. VAPB depletion alters neuritogenesis and phosphoinositide balance in motoneuron-like cells: relevance to VAPB-linked amyotrophic lateral sclerosis. J Cell Sci. 2019;132(7).
74. Van Harten ACM, Phatnani H, Przedborski S. Non-cell-autonomous pathogenic mechanisms in amyotrophic lateral sclerosis. Trends Neurosci. 2021;44(8):658-68.
75. Philips T, Rothstein JD. Glial cells in amyotrophic lateral sclerosis. Exp Neurol. 2014;262 Pt B:111-20.

76. Cappello V, Francolini M. Neuromuscular Junction Dismantling in Amyotrophic Lateral Sclerosis. Int J Mol Sci. 2017;18(10).
77. Mejzini R, Flynn LL, Pitout IL, Fletcher S, Wilton SD, Akkari PA. ALS Genetics, Mechanisms, and Therapeutics: Where Are We Now? Front Neurosci. 2019;13:1310.
78. Le Gall L, Anakor E, Connolly O, Vijayakumar UG, Duddy WJ, Duguez S. Molecular and Cellular Mechanisms Affected in ALS. J Pers Med. 2020;10(3).
79. Wijesinghe R, Camp AJ. Intrinsic neuronal excitability: implications for health and disease. Biomol Concepts. 2011;2(4):247-59.
80. Falco-Walter J. Epilepsy-Definition, Classification, Pathophysiology, and Epidemiology. Semin Neurol. 2020;40(6):617-23.
81. Kazim SF, Seo JH, Bianchi R, Larson CS, Sharma A, Wong RKS, et al. Neuronal Network Excitability in Alzheimer's Disease: The Puzzle of Similar versus Divergent Roles of Amyloid β and Tau. eNeuro. 2021;8(2).
82. Pieri M, Albo F, Gaetti C, Spalloni A, Bengtson CP, Longone P, et al. Altered excitability of motor neurons in a transgenic mouse model of familial amyotrophic lateral sclerosis. Neurosci Lett. 2003;351(3):153-6.
83. Kuo JJ, Schonewille M, Siddique T, Schults AN, Fu R, Bär PR, et al. Hyperexcitability of cultured spinal motoneurons from presymptomatic ALS mice. J Neurophysiol. 2004;91(1):571-5.
84. Kuo JJ, Siddique T, Fu R, Heckman CJ. Increased persistent Na(+) current and its effect on excitability in motoneurones cultured from mutant SOD1 mice. J Physiol. 2005;563(Pt 3):843-54.
85. Wainger BJ, Kiskinis E, Mellin C, Wiskow O, Han SS, Sandoe J, et al. Intrinsic membrane hyperexcitability of amyotrophic lateral sclerosis patient-derived motor neurons. Cell Rep. 2014;7(1):1-11.
86. Gunes ZI, Kan VWY, Ye X, Liebscher S. Exciting Complexity: The Role of Motor Circuit Elements in ALS Pathophysiology. Front Neurosci. 2020;14:573.
87. Fogarty MJ. Driven to decay: Excitability and synaptic abnormalities in amyotrophic lateral sclerosis. Brain Res Bull. 2018;140:318-33.
88. Gunasekaran R, Narayani RS, Vijayalakshmi K, Alladi PA, Shobha K, Nalini A, et al. Exposure to cerebrospinal fluid of sporadic amyotrophic lateral sclerosis patients alters Nav1.6 and Kv1.6 channel expression in rat spinal motor neurons. Brain Res. 2009;1255:170-9.

89. Pieri M, Carunchio I, Curcio L, Mercuri NB, Zona C. Increased persistent sodium current determines cortical hyperexcitability in a genetic model of amyotrophic lateral sclerosis. Exp Neurol. 2009;215(2):368-79.
90. Kiskinis E, Sandoe J, Williams LA, Boulting GL, Moccia R, Wainger BJ, et al. Pathways disrupted in human ALS motor neurons identified through genetic correction of mutant SOD1. Cell Stem Cell. 2014;14(6):781-95.
91. Saba L, Viscomi MT, Martini A, Caioli S, Mercuri NB, Guatteo E, et al. Modified age-dependent expression of NaV1.6 in an ALS model correlates with motor cortex excitability alterations. Neurobiol Dis. 2019;130:104532.
92. Urbani A, Belluzzi O. Riluzole inhibits the persistent sodium current in mammalian CNS neurons. Eur J Neurosci. 2000;12(10):3567-74.
93. Cheah BC, Vucic S, Krishnan AV, Kiernan MC. Riluzole, neuroprotection and amyotrophic lateral sclerosis. Curr Med Chem. 2010;17(18):1942-199.
94. Bellingham MC. A review of the neural mechanisms of action and clinical efficiency of riluzole in treating amyotrophic lateral sclerosis: what have we learned in the last decade? CNS Neurosci Ther. 2011;17(1):4-31.
95. Chen JJ. Overview of current and emerging therapies for amytrophic lateral sclerosis. Am J Manag Care. 2020;26(9 Suppl):S191-S7.
96. Van Damme P, Robberecht W, Van Den Bosch L. Modelling amyotrophic lateral sclerosis: progress and possibilities. Dis Model Mech. 2017;10(5):537-49.
97. Morrice JR, Gregory-Evans CY, Shaw CA. Animal models of amyotrophic lateral sclerosis: A comparison of model validity. Neural Regen Res. 2018;13(12):2050-4.
98. Gois AM, Mendonça DMF, Freire MAM, Santos JR. IN VITRO AND IN VIVO MODELS OF AMYOTROPHIC LATERAL SCLEROSIS: AN UPDATED OVERVIEW. Brain Res Bull. 2020;159:32-43.
99. Bonifacino T, Zerbo RA, Balbi M, Torazza C, Frumento G, Fedele E, et al. Nearly 30 Years of Animal Models to Study Amyotrophic Lateral Sclerosis: A Historical Overview and Future Perspectives. Int J Mol Sci. 2021;22(22).
100. Raimondi A, Mangolini A, Rizzardini M, Tartari S, Massari S, Bendotti C, et al. Cell culture models to investigate the selective vulnerability of motoneuronal mitochondria to familial ALS-linked G93ASOD1. Eur J Neurosci. 2006;24(2):387-99.
101. Smith RS, Walsh CA. Ion Channel Functions in Early Brain Development. Trends Neurosci. 2020;43(2):103-14.

102. Maier O, Böhm J, Dahm M, Brück S, Beyer C, Johann S. Differentiated NSC-34 motoneuron-like cells as experimental model for cholinergic neurodegeneration. Neurochem Int. 2013;62(8):1029-38.
103. Moreno-Ortega AJ, Al-Achbili LM, Alonso E, de Los Ríos C, García AG, Ruiz-Nuño A, et al. Neuroprotective Effect of the Novel Compound ITH33/IQM9.21 Against Oxidative Stress and Na(+) and Ca(2+) Overload in Motor Neuron-like NSC-34 Cells. Neurotox Res. 2016;30(3):380-91.
104. Mouhid Al-Achbili L, Moreno-Ortega AJ, Matías-Guiu J, Cano-Abad MF, Ruiz-Nuño A. ITH33/IQM9.21 provides neuroprotection in a novel ALS model based on TDP-43 and Na. Neurosci Lett. 2016;633:28-32.
105. Silbernagel N, Walecki M, Schäfer MK, Kessler M, Zobeiri M, Rinné S, et al. The VAMP-associated protein VAPB is required for cardiac and neuronal pacemaker channel function. FASEB J. 2018;32(11):6159-73.
106. McGuirt AF, Post MR, Pigulevskiy I, Sulzer D, Lieberman OJ. Coordinated Postnatal Maturation of Striatal Cholinergic Interneurons and Dopamine Release Dynamics in Mice. J Neurosci. 2021;41(16):3597-609.
107. Nango H, Kosuge Y, Sato M, Shibukawa Y, Aono Y, Saigusa T, et al. Highly Efficient Conversion of Motor Neuron-Like NSC-34 Cells into Functional Motor Neurons by Prostaglandin E. Cells. 2020;9(7).
108. Hsia HE, Kumar R, Luca R, Takeda M, Courchet J, Nakashima J, et al. Ubiquitin E3 ligase Nedd4-1 acts as a downstream target of PI3K/PTEN-mTORC1 signaling to promote neurite growth. Proc Natl Acad Sci U S A. 2014;111(36):13205-10.
109. Durak O, de Anda FC, Singh KK, Leussis MP, Petryshen TL, Sklar P, et al. Ankyrin-G regulates neurogenesis and Wnt signaling by altering the subcellular localization of β-catenin. Mol Psychiatry. 2015;20(3):388-97.
110. Marcuzzo S, Terragni B, Bonanno S, Isaia D, Cavalcante P, Cappelletti C, et al. Hyperexcitability in Cultured Cortical Neuron Networks from the G93A-SOD1 Amyotrophic Lateral Sclerosis Model Mouse and its Molecular Correlates. Neuroscience. 2019;416:88-99.
111. Bonnevie VS, Dimintiyanova KP, Hedegaard A, Lehnhoff J, Grøndahl L, Moldovan M, et al. Shorter axon initial segments do not cause repetitive firing impairments in the adult presymptomatic G127X SOD-1 Amyotrophic Lateral Sclerosis mouse. Sci Rep. 2020;10(1):1280.

112. Jørgensen HS, Jensen DB, Dimintiyanova KP, Bonnevie VS, Hedegaard A, Lehnhoff J, et al. Increased Axon Initial Segment Length Results in Increased Na. Neuroscience. 2021;468:247-64.
113. Osking Z, Ayers JI, Hildebrandt R, Skruber K, Brown H, Ryu D, et al. ALS-Linked SOD1 Mutants Enhance Neurite Outgrowth and Branching in Adult Motor Neurons. iScience. 2019;11:294-304.
114. Munnamalai V, Suter DM. Reactive oxygen species regulate F-actin dynamics in neuronal growth cones and neurite outgrowth. J Neurochem. 2009;108(3):644-61.
115. Rátkai A, Tárnok K, Aouad HE, Micska B, Schlett K, Szücs A. Homeostatic plasticity and burst activity are mediated by hyperpolarization-activated cation currents and T-type calcium channels in neuronal cultures. Sci Rep. 2021;11(1):3236.
116. De Matteis MA, Rega LR. Endoplasmic reticulum-Golgi complex membrane contact sites. Curr Opin Cell Biol. 2015;35:43-50.
117. Phillips MJ, Voeltz GK. Structure and function of ER membrane contact sites with other organelles. Nat Rev Mol Cell Biol. 2016;17(2):69-82.
118. Navone F, Genevini P, Borgese N. Autophagy and Neurodegeneration: Insights from a Cultured Cell Model of ALS. Cells. 2015;4(3):354-86.
119. Anagnostou G, Akbar MT, Paul P, Angelinetta C, Steiner TJ, de Belleroche J. Vesicle associated membrane protein B (VAPB) is decreased in ALS spinal cord. Neurobiol Aging. 2010;31(6):969-85.
120. Mitne-Neto M, Machado-Costa M, Marchetto MC, Bengtson MH, Joazeiro CA, Tsuda H, et al. Downregulation of VAPB expression in motor neurons derived from induced pluripotent stem cells of ALS8 patients. Hum Mol Genet. 2011;20(18):3642-52.
121. Mao D, Lin G, Tepe B, Zuo Z, Tan KL, Senturk M, et al. VAMP associated proteins are required for autophagic and lysosomal degradation by promoting a PtdIns4P-mediated endosomal pathway. Autophagy. 2019;15(7):1214-33.
122. Di Paolo G, De Camilli P. Phosphoinositides in cell regulation and membrane dynamics. Nature. 2006;443(7112):651-7.
123. Ling Y, Hayano S, Novick P. Osh4p is needed to reduce the level of phosphatidylinositol-4-phosphate on secretory vesicles as they mature. Mol Biol Cell. 2014;25(21):3389-400.
124. D'Avanzo N, McCusker EC, Powl AM, Miles AJ, Nichols CG, Wallace BA. Differential lipid dependence of the function of bacterial sodium channels. PLoS One. 2013;8(4):e61216.

125. Braun C, Parks XX, Qudsi H, Lopes CMB. Membrane pools of phosphatidylinositol-4-phosphate regulate KCNQ1/KCNE1 membrane expression. Commun Biol. 2021;4(1):1392.
126. Rabinovich-Toidman P, Rabinovich-Nikitin I, Ezra A, Barbiro B, Fogel H, Slutsky I, et al. Mutant SOD1 Increases APP Expression and Phosphorylation in Cellular and Animal Models of ALS. PLoS One. 2015;10(11):e0143420.
127. Brocard C, Plantier V, Boulenguez P, Liabeuf S, Bouhadfane M, Viallat-Lieutaud A, et al. Cleavage of Na(+) channels by calpain increases persistent Na(+) current and promotes spasticity after spinal cord injury. Nat Med. 2016;22(4):404-11.
128. Plantier V, Sanchez-Brualla I, Dingu N, Brocard C, Liabeuf S, Gackière F, et al. Calpain fosters the hyperexcitability of motoneurons after spinal cord injury and leads to spasticity. Elife. 2019;8.
129. de la Fuente S, Sansa A, Hidalgo I, Vivancos N, Romero-Guevara R, Garcera A, et al. Calpain system is altered in survival motor neuron-reduced cells from in vitro and in vivo spinal muscular atrophy models. Cell Death Dis. 2020;11(6):487.

List of figures and tables

Dissemination of results

The results described in this thesis will be part of a publication in a peer reviewed journal in order to disseminate the results to the scientific community.
During the three years of the PhD the data were presented in different national and international congress:
-Brayn conference 2019 – Poster presentation
- FEBS Congress 2021 – Poster presentation
- Workshop BIOMETRA 2021 – Poster presentation

Short lay summary

During the three years of my PhD I focused my attention in the study of motorneuron, a specialize cell of the central nervous system that carry movements signals from our brain throughout the body conducting an electric impulse. To generate and conduct the electric impulse this specialize cells express in their membrane ionic channels: transmembrane protein that create and control a hole in the membrane leading the passage of electric charges. I focused my attention on the study of the ion channels responsible for the maintaining of the excitation state of neuron to understand if they are involved in the pathogenesis of the Amyotrophic Lateral Sclerosis, a devastating disease that cause paralysis and death within 2-5 year from the diagnosis.

Durante i tre anni di studio del mio dottorato ho focalizzato la mia attenzione nello studio dei motoneuroni, cellule specializzate del sistema nervoso centrale che sono responsabili di trasmettere segnali motori dal nostro cervello attraverso tutto il corpo conducendo un impulso nervoso. Per generare e condurre questo impulso queste cellule specializzate esprimono nella loro membrana dei canali ionici: proteine transmembrana che creano e controllano un foro nella membrana permettendo il passaggio di cariche elettriche. Ho focalizzato la mia attenzione nello studio dei canali ionici responsabili del mantenimento dello stato di eccitazione dei neuroni per cercare di comprendere se questi canali sono coinvolti nella patogenesi della Sclerosi Laterale Amiotrofica, una patologia devastante che causa la paralisi e la morte del paziente in 2-5 anni dalla diagnosi.